Current Research in Immunology 1 (2020) 23–37

Contents lists available at ScienceDirect

Current Research in Immunology

journal homepage: www.editorialmanager.com/crimmu/Default.aspx

Impact of IgG1 N-glycosylation on their interaction with Fc gamma receptors

Florian Cambay [a,b], Céline Raymond [b,c,1], Denis Brochu [d], Michel Gilbert [d], The Minh Tu [b], Christiane Cantin [b], Anne Lenferink [b], Maxime Grail [a], Olivier Henry [a], Gregory De Crescenzo [a,*], Yves Durocher [b,c,**]

[a] Department of Chemical Engineering, Polytechnique Montréal, Montreal, Canada
[b] Human Health Therapeutics Research Centre, National Research Council of Canada, Montreal, Canada
[c] Department of Biochemistry and Molecular Medicine, University of Montreal, Montreal, Canada
[d] Human Health Therapeutics Research Centre, National Research Council of Canada, Ottawa, Canada

ARTICLE INFO

Keywords:
N-glycosylation
IgG1
Fcγ receptors
Surface plasmon resonance

ABSTRACT

The effector functions of the IgGs are modulated by the N-glycosylation of their Fc region. Particularly, the absence of core fucosylation is known to increase the affinity of IgG1s for the Fcγ receptor IIIa expressed by immune cells, in turn translating in an improvement in the antibody-dependent cellular cytotoxicity. However, the impact of galactosylation and sialylation is still debated in the literature. In this study, we have investigated the influence of high and low levels of core fucosylation, terminal galactosylation and terminal α2,6-sialylation of the Fc N-glycans of trastuzumab on its affinity for the FcγRIIIa. A large panel of antibody glycoforms (i.e., highly α2,6-sialylated or galactosylated IgG1s, with high or low levels of core fucosylation) were generated and characterized, while their interactions with the FcγRs were analysed by a robust surface plasmon resonance-based assay as well as in a cell-based reporter bioassay. Overall, IgG1 glycoforms with reduced fucosylation display a stronger affinity for the FcγRIIIa. In addition, fucosylation, and the presence of terminal galactose and sialic acids are shown to increase the affinity for the FcγRIIIa as compared to the agalactosylated forms. These observations perfectly translate in the response observed in our reporter bioassay.

Introduction

Monoclonal antibodies (mAbs) represent a major class of biotherapeutics. They are mostly recombinant IgG1 produced in Chinese hamster ovary (CHO) cells (Walsh, 2018). Their efficacy relies in part on the ability to trigger cellular effector functions by binding, through their Fc region, to the Fcγ receptors (FcγRs) present at the surface of the immune cells (Jiang et al., 2011). There are three distinct types of FcγRs: the type I receptor (FcγRI) which is a high affinity receptor for human IgG1s (hIgG1s) (apparent K_D of $10^{-8} - 10^{-9}$ M) while the type II (FcγRIIa-c) and type III (FcγRIIIa/b) receptors display much lower affinities (apparent K_Ds of $\approx 10^{-6} - 10^{-7}$ M) (Bruhns et al., 2009; Lu et al., 2015). The triggering of cellular effector functions such as antibody-dependent cellular phagocytosis (ADCP), and antibody-dependent cellular cytotoxicity (ADCC) depends on the immune cells and the type(s) of FcγRs they express and that are involved in the interaction with the Fc region of a hIgG1. The ADCC is mediated by the interaction of a hIgG1-Fc with the activating FcγRIIIa expressed on the cell surface of primarily natural killer (NK) cells, although monocytes, macrophages, neutrophils, eosinophils and dendritic cells also express this receptor. The FcγRIIIa has two polymorphic variants, with the residue at position 158 either being a valine (V158) or a phenylalanine (F158), with the V158 variant displaying a much higher affinity for hIgG1s than the F158 variant (Bruhns et al., 2009; Dekkers et al., 2017). The expression of the high-affinity V158 variant (genotype V/V158) is present in ~10–15%, while the low-affinity F158 variant is found in >85% of the population (genotypes V/F158 or F/F158). Of these variants, the V/V158 genotype has been associated *in vivo* with a better anti-CD20 antibody-induced ADCC (Cartron et al., 2002).

Human IgG1 possesses two N-glycans on the asparagine 297 of each of the heavy chain and their presence are necessary for Fc binding to

* Corresponding author.
** Corresponding author. Human Health Therapeutics Research Centre, National Research Council Canada, 6100 Royalmount, Montreal, QC, H4P 2R2, Canada.
E-mail addresses: gregory.decrescenzo@polymtl.ca (G. De Crescenzo), Yves.Durocher@cnrc-nrc.gc.ca (Y. Durocher).
[1] Present address: Merck Biodevelopment, 33650 Martillac, France.

https://doi.org/10.1016/j.crimmu.2020.06.001
Received 10 March 2020; Received in revised form 1 June 2020; Accepted 2 June 2020

Abbreviations

ADCC	antibody-dependent cell-mediated cytotoxicity
ADCP	antibody-dependent cellular phagocytosis
CDC	complement-dependent cytotoxicity
EBNA1	Epstein-Barr virus Nuclear Antigen-1
ECL	*Erythrina cristagalli* lectin
FcγR	Fcγ receptor
FUT8	fucosyltransferase VIII
GnTIII	β-1,4-N-acetylglucosaminyltransferase
GT	human glycosyltransferase β1,4-galactosyltransferase 1
GTS	GDP-6-deoxy-D-talose synthetase
HC	heavy chain
HRP	horseradish peroxidase
LC	light chain
LCA	*Lens culinaris* agglutinin
MALII	*Maackia amurensis* lectin II
NK	natural killer
RMD	GDP-4-dehydro-6-deoxy-D-mannose reductase
SNA	*Sambucus nigra agglutinin*
ST6Gal1	β-galactoside α2,6-sialyltransferase 1
TZM	trastuzumab

FcγRIIIa (Dorion-Thibaudeau et al., 2014, 2016; Yamaguchi et al., 2006). Moreover, the affinity of hIgG1s for both FcγRIIIa variants is particularly sensitive to the absence of fucosylation on the Fc N297 glycan, which drastically increases its affinity for the FcγRIIIa receptor (Shields et al., 2002; Shinkawa et al., 2003) and translates in an increased capacity to elicit an ADCC response (Shields et al., 2002). This interaction is particularly complex, as it depends on protein-protein, protein-glycan and glycan-glycan contacts (Ferrara et al., 2011; Mizushima et al., 2011). More precisely, the FcγRIIIa N162 glycan is directly involved in the interaction with the afucosylated hIgG1 (Ferrara et al., 2011) while other studies have also highlighted the influence of FcγRIIIa N-glycans on IgG1 binding kinetics (Hayes et al., 2017; Zeck et al., 2011; Edberg and Kimberly, 1997; Subedi and Barb, 2018). Over 70% of all hIgG1s in circulation are fucosylated and the cells used for the production of recombinant protein mainly produce highly fucosylated IgG1s. For example, fucosylation levels of 90–95% is typically achieved in CHO cell-produced IgG1s (Arnold et al., 2007; Raju, 2008). Therefore, afucosylated antibodies must be obtained through process and cellular engineering strategies. These include kifunensine supplementation (van Berkel et al., 2010), GDP-fucose synthesis-defective cells (CHO Lec13) (Shields et al., 2002), the use of fucosyltransferase VIII (FUT8) gene knockout cells (Yamane-Ohnuki et al., 2004), FUT8 inhibitors (Rillahan et al., 2012), and through the co-expression of β-1,4-N-acetylglucosaminyltransferase (GnTIII) and Golgi α-mannosidase (ManII) (Ferrara et al., 2006a) or enzymes deflecting the GDP-fucose biosynthesis pathway (e.g., bacterial GDP-6-deoxy-D-talose synthetase [GTS] or GDP-6-deoxy-D-lyxo-4-hexulose reductase [RMD]) (von Horsten et al., 2010; Kelly et al., 2018).

Unlike fucosylation, the respective effects of terminal galactose or sialic acid on FcγR binding are still rather ambiguous. For example it has been reported that differences in terminal galactosylation levels do not correlate with an increased ADCC activity (Shinkawa et al., 2003; Boyd et al., 1995) whereas other studies described a positive influence (Dekkers et al., 2017; Thomann et al., 2015; Wada et al., 2019). In parallel, several recent studies have demonstrated the beneficial effect of terminal galactose on the affinity of hIgG1 for the FcγRIIIa as well as other low-affinity FcγRs (Dekkers et al., 2017; Yamaguchi et al., 2006; Dorion-Thibaudeau et al., 2016; Thomann et al., 2015; Wada et al., 2019; Ahmed et al., 2014; Subedi and Barb, 2016; Dashivets et al., 2015). In contrast, interactions with FcγRI were reported to be unaffected by the IgG1 N-glycan variations (Dekkers et al., 2017; Thomann et al., 2015; Subedi and Barb, 2016; Dashivets et al., 2015).

Terminal sialylation may confer anti-inflammatory properties to hIgG1s while reducing their affinity for FcγRIIIa and their ability to induce ADCC activity (Dekkers et al., 2017; Kaneko et al., 2006; Anthony et al., 2008; Li et al., 2017). This negative correlation between sialylation and FcγRIIIa binding has also been observed by others (Wada et al., 2019; Scallon et al., 2007; Naso et al., 2010). In contrast, some recent studies reported that α2,6-sialylation has almost no influence on IgG1/FcγRIIIa interactions when compared to hIgG1 galactosylation (Thomann et al., 2015; Subedi and Barb, 2016; Dashivets et al., 2015; Peipp et al., 2008; Shivatare et al., 2018). On the other hand, it has been suggested that galactosylation and sialylation positively influences the complement-dependent cytotoxicity (CDC) response (Dekkers et al., 2017; Wada et al., 2019; Peschke et al., 2017). In CHO cells, glycoproteins are typically undergalactosylated and only traces of sialic acids can be detected (Jefferis, 2009). In addition, given that N-glycosylation is cell-type dependent, specific glycan epitopes can be favoured depending on the expression system used. For example, N-glycans from CHO cells display only α2,3-sialylation whereas α2,6- and to a lesser extent α2,3-sialylation are found in mouse and human cell lines (Arnold et al., 2007; Anthony et al., 2008; Lee et al., 1989; Durocher and Butler, 2009; Lalonde and Durocher, 2017).

Three major approaches have been used to enhance the terminal galactosylation and α2,6-sialylation of hIgG1s: (i) *in vitro* enzymatic glycan remodelling, (ii) chemoenzymatic glycoengineering and, (iii) transient over-expression of glycosyltransferases such as β4GT1 and ST6Gal1. The *in vitro* enzymatic addition of galactose and sialic acid residues is very time-consuming and expensive (Yamaguchi et al., 2006; Thomann et al., 2015; Subedi and Barb, 2016; Dashivets et al., 2015; Anthony et al., 2008; Peipp et al., 2008; Peschke et al., 2017; Barb et al., 2012; Raju et al., 2001) compared to chemoenzymatic glycoengineering that also leads to well-defined homogeneous product glycoforms (Wada et al., 2019; Li et al., 2017; Shivatare et al., 2018; Kurogochi et al., 2015; Lin et al., 2015; Tsukimura et al., 2017). Lastly, glycoengineering by transient over-expression of human β4GT1 and ST6Gal1 allows for a fast production of hIgG1s enriched in galactose and α2,6-sialylated residues (Raymond et al., 2015; Dekkers et al., 2016).

To unravel the influence of IgG1-Fc N-glycans on their affinity for the FcγRs, we generated eight hIgG1 Trastuzumab (TZM) glycovariants displaying well-characterized levels of core fucose, terminal galactosylation and terminal α2,6-sialylation on the N-glycans present in the IgG1's Fc portion. These TZM glycoforms were produced in CHO cells by transient co-expression of various combinations of human β4GT1 and ST6Gal1, and bacterial GDP-6-deoxy-D-lyxo-4-hexulose reductase (RMD), as well as *in vitro* sialylation using a soluble human ST6Gal1 construct. TZM glycoprofiles were characterized by lectin blots, capillary isoelectric focusing (cIEF) and hydrophilic interaction chromatography (HILIC), while binding to the FcγRs was analysed through a robust SPR-based assay (Cambay et al., 2019) and a cell-based reporter bioassay.

Materials and methods

Cell lines

The Chinese hamster ovary-3E7 (CHO-3E7) and the human embryonic kidney 293-6E (293-6E) cell lines, stably expressing a truncated Epstein-Barr virus Nuclear Antigen-1 (EBNA1), were cultured as described elsewhere (Cambay et al., 2019).

Production and purification of TZM glycoforms

TZM is a humanized mouse IgG1 directed against the human epidermal growth factor receptor-2 (HER2 or Erb2). TZM glycoforms were produced by transient gene expression in CHO-3E7 cells. The light and heavy chains of TZM were each cloned into pTT5® vectors (Zhang

et al., 2009), as well as the human glycosyltransferases β1,4-galactosyltransferase 1 (GT), β-galactoside α-2,6-sialyltransferase 1 (ST6), and the bacterial enzyme GDP-6-deoxy-D-lyxo-4-hexulose reductase (RMD). When GT, ST6 or RMD were required, the DNA transfection mixes contained 5%, 20% and 5% in weight of GT, ST6 and RMD plasmids, respectively. The pTT® vector encoding the green fluorescent protein (GFP) was used to monitor transfection efficiency as described elsewhere (Durocher et al., 2002). GFP plasmid was incorporated as 5% in weight for all transfections. The pTT22®-AKT-DD plasmid is derived from the pTT® vector and encodes constitutively active bovine AKT (Alessi et al., 1996). AKT plasmid was incorporated as 15% in weight for all transfections. The remaining of the DNA mix was a mixture of LC and HC plasmids (LC:HC ratio of 6:4). Linear deacylated polyethylenimine (L-PEImax) was from Polysciences (cat# 24765) as sterile stock solutions in water (1 mg/mL) and stored at 4 °C. Cells were diluted two days before transfection in fresh medium at 0.25 × 10^6 cells/mL. They were transfected with viability greater that 99% at densities between 1.5 and 2.0 × 10^6 cells/mL. DNA and L-PEImax solutions were separately prepared in complete F17 medium for a final concentration of 1 μg/mL and 5 μg/mL, respectively in the final culture volume, then L-PEImax was added to DNA. The mixtures were immediately vortexed and incubated for 5 min at room temperature prior to addition to the cells. One day post-transfection (dpt), cells were fed with TN1 peptone and valproic acid to final concentrations of 1% (w/v) and 0.5 mM, respectively. The temperature was shifted to 32 °C and the glucose concentration was adjusted to a final concentration of 30 mM. Transfection efficiency was assessed two dpt by determining the percentage of GFP-positive cells using a Cellometer® K2 (Nexcelom Bioscience). Four dpt, cell cultures were centrifuged at 3300×*g* for 20 min at a viability higher than 80%. Supernatants were then filtered through 0.45 μm membranes and the clarified supernatants were purified by affinity chromatography with MabSelect™ SuRe™ columns (GE Healthcare, cat# 17-5438-02) followed by size exclusion chromatography (SEC) using a Superdex200 column (GE Healthcare, cat# 28-9893-35) to remove aggregates as explained elsewhere (Cambay et al., 2019). The final yields ranged from 4.7 to 59.8 mg/L.

Production and purification of FcγRs

E5-tagged FcγRs were produced by transient gene expression in CHO-3E7 and 293-6E then purified by immobilized metal-affinity chromatography (IMAC) followed by size exclusion chromatography (SEC) as described elsewhere (Cambay et al., 2019). Concerning the E5-tagged FcγRIIa/b and FcγRI, their purification characterization is given in Supplementary Fig. S2.

Production and purification of soluble ST6Gal1

DNA encoding the truncated human ST6Gal1 lacking the N-terminal cytoplasmic tail and the transmembrane domain was inserted into a pTT5® vector. The truncated ST6Gal1 sequence was flanked by a signal peptide from the vascular endothelial growth factor A for secretion and a 10-histidine tag inserted at the C-terminus to facilitate its purification. Soluble ST6Gal1 were produced by transient expression in 293-6E cells at 37 °C. Cell cultures were harvested 5 dpt, centrifuged at 3300×*g* for 20 min and supernatants were filtered through 0.45 μm membranes. The clarified supernatants were purified by immobilized metal-affinity chromatography (IMAC) with 4 mL Ni Sepharose® Excel columns (GE Healthcare, cat# 17-3712-03). The columns were washed with sodium phosphate 50 mM, 300 mM NaCl, pH 7.0 and the ST6Gal1 were eluted with the washing buffer containing imidazole (500 mM), pH 7.0. The fractions containing the ST6Gal1 were pooled and the elution buffer was exchanged against PBS with a CentriPure P100 column (Emp Biotech, cat# CP-0119-Z001.0–001). Purified ST6Gal1 was finally quantified by absorbance at 280 nm using a Nanodrop™ spectrophotometer (Thermo Fisher Scientific) based on its molar extinction coefficient, sterile-filtered, aliquoted and stored at −80 °C.

In vitro sialylation (IVS)

The *in vitro* sialylation method was adapted from the protocol published by Barb et al. (2012). An enzyme:antibody ratio of 1:6 (w/w) was used. The antibody (1–1.5 mg/mL) was sialylated with ST6Gal1 in presence of CMP-N-acetylneuraminic acid (CMP-NANA - Roche, cat# 05974003103) at 1 mM in 25 mM MOPS buffer, KCl 100 mM, pH 7.2 at 37 °C. After 24 h, the reaction mixture was concentrated 10-fold on Amicon Ultra-15 mL with a 3 kDa cut-off (Millipore, cat# UFC900308) to eliminate the free CMP. The volume was readjusted to its initial value and a fresh aliquot of CMP-NANA was added to a final concentration of 1 mM. This 24-h cycle was repeated three times. At the end of the fourth day, the reaction mixture was loaded on a 1 mL MabSelect™ SuRe™ column and the antibody was purified as described above.

Coomassie-stained gels and lectin blots

The proteins were loaded on NuPAGE Novex 4–12% gels from Life sciences (cat#NP0323BOX) ran in MES buffer (Novex) at 170 V for 60 min. For the Coomassie staining, 1.5 μg of protein per well were loaded. The gels were stained with Coomassie Brilliant Blue for 15 min then destained overnight in a solution of acetic acid 7.5% (v:v) and ethanol 20% (v:v). For lectin blots, biotinylated lectins *Sambucus nigra* agglutinin (SNA), *Erythrina cristagalli* lectin (ECL), *Maackia amurensis* lectin II (MALII) and *Lens culinaris* agglutinin (LCA) were purchased from Vector Laboratories (cat# SNA: B-1305, ECL: B-1145, MALII: B-1265, LCA: B-1045). Samples were treated with DTT (10 min at 70 °C) and 120 ng of purified mAbs were loaded on the gels for SNA blots and 180 ng for the other lectin blots. After protein transfer, the nitrocellulose membrane was incubated 1 h in blocking reagent, then with a given lectin for 2 h (5 μg/mL ECL, 5 μg/mL MALII, 2 μg/mL SNA or 10 μg/mL LCA), followed by incubation with 1:1000 Streptavidin-HRP (BD Biosciences, cat# 554066) for 1 h. The membranes were thoroughly washed with PBS-Tween 0.1% before each incubation step. Ponceau red staining was performed to control the amount of protein loaded. Signal was revealed with the ImmunStar™ Western C™ Substrate Kit (Bio-Rad, cat# 170–5070) and the images recorded with a Chemidoc MP Imaging System (Bio-Rad).

Capillary isoelectric focusing (cIEF)

Separations were performed on Agilent 7100 Capillary Electrophoresis systems (Agilent Technologies) with the detector filter G7100-68750 at 280 nm. Typically, a capillary with a 33 cm total length (24 cm effective length) was pre-conditioned at 3.5 bar for 5 min with 0.5% methyl cellulose, then for 3 min with 4.3 M urea and finally for 2 min with dH_2O prior to injection. Each injection was performed for 100 s at 3.5 bar. Then, the capillary inlet and outlet were dipped into 200 mM phosphoric acid and 300 mM NaOH respectively and the focusing was performed for 5 min at + 25 kV. After 5 min, the capillary outlet was dipped into dH2O then into 350 mM acetic acid and the chemical mobilization was performed for 25 min at + 30 kV. Each run was repeated three times. The samples were prepared as followed: 5 μg of TZM glycoforms were mixed with 0.6% methyl cellulose in 3 M urea, L-Arginine, iminodiacetic acid, DPBS and 2 pI markers mixed (3.59 and 10). The apparent pIs were determined based on the 2 pI markers.

Hydrophilic interaction liquid chromatography (HILIC)

Glycans were released from the antibody using Rapid™ PNGase F (New England BioLabs, cat# P0710) at 37 °C for 24 h. The enzyme and the antibody were removed using prewashed 10 kDa molecular weight cut-off filters, and the glycans were evaporated to dryness under vacuum. They were then labelled with 2-aminobenzamide (2-AB) (Sigma-Aldrich,

cat# PP0520) (Bigge et al., 1995). Glycans were analysed by HILIC with fluorescent detection using a TSKgel® Amide-80 4.6 × 150 mm, 3.0 μm (Tosoh Biosciences, cat# 0021867) with the column heated to 45 °C and a flow rate of 0.5 mL/min. Glycans were eluted using 100 mM ammonium formate, pH 4.5 (mobile phase A) and 100% acetonitrile (mobile phase B) starting with an initial ratio of 25:75, followed by a gradient to 50:50 over 50 min. Peaks were calibrated with a 2-AB labelled dextran ladder standard (Agilent, cat# 5190–6998) and compared to GU values in the database Glycobase. NIBRT (https://glycobase.nibrt.ie/glycobase/show_nibrt.action). Structural assignment was also based on exoglycosidase analysis (Royle et al., 2007). Broad specificity Neuraminidase (MP biomedicals cat# 153846) and Sialidase S (Prozyme, cat# GK80020) were used for sialic acid digests according to the manufacturer's instructions. The glycans abundance was calculated based on the peak areas observed in the chromatograms. The percentage of a given glycan was obtained as the peak area of the PNGaseF released glycan divided by the sum of the areas of all the peaks detected in the chromatogram. These percentages were then compiled by glycan families using the following terms:

%fucosylated = 100 * (%G0F + %G1Fa + %G1Fb + %G2F + %G1FS(3)1 + %G1FS(6)1 + %G2FS(3)1 + %G2FS(6)1 + %G2FS(3,3)2 + %G2FS(3,6)2 + %G2FS(6,6)2) / (%G0F + %G1Fa + %G1Fb + %G2F + %G0 + %G1a + %G1b + %G2 + %G1FS(3)1 + %G1FS(6)1 + %G2FS(3)1 + %G2FS(6)1 + %G2FS(3,3)2 + %G2FS(3,6)2 + %G2FS(6,6)2 + %G2S(6)1 + %G2S(6,6)2)

%agalactosylated = 100 * (2 * %G0F + 1 * %G1Fa + 1 * %G1Fb + 2 * %G0 + 1 * %G1a +1 * %G1b + 1 * %G1FS(3)1 + 1 * %G1FS(6)1) / (2 * %G0F + 2 * %G1Fa + 2 * %G1Fb + 2 * %G2F + 2 * %G0 + 2 * %G1a +2 * %G1b + 2 * %G2 + 2 * %G1FS(3)1 + 2 * %G1FS(6)1 + 2 * %G2FS(3)1 + 2 * %G2FS(6)1 + 2 * %G2FS(3,3)2 + 2 * %G2FS(3,6)2 + 2 * %G2FS(6,6)2 + 2 * %G2S(6)1 + 2 * %G2S(6,6)2)

%galactosylated = 100 * (1 * %G1Fa + 1 * %G1Fb + 2 * %G2F + 1 * %G1a +1 * %G1b + 2 * %G2 + 1 * %G2FS(3)1 + 1 * %G2FS(6)1 + 1 * %G2S(6)1) / (2 * %G0F + 2 * %G1Fa + 2 * %G1Fb + 2 * %G2F + 2 * %G0 + 2 * %G1a +2 * %G1b + 2 * %G2 + 2 * %G1FS(3)1 + 2 * %G1FS(6)1 + 2 * %G2FS(3)1 + 2 * %G2FS(6)1 + 2 * %G2FS(3,3)2 + 2 * %G2FS(3,6)2 + 2 * %G2FS(6,6)2 + 2 * %G2S(6)1 + 2 * %G2S(6,6)2)

%sialylated = 100 * (1 * %G1FS(3)1 + 1 * %G1FS(6)1 + 1 * %G2FS(3)1 + 1 * %G2FS(6)1 + 2 * %G2FS(3,3)2 + 2 * %G2FS(3,6)2 + 2 * %G2FS(6,6)2 + 1 * %G2S(6)1 + 2 * %G2S(6,6)2) / (1 * %G1Fa + 1 * %G1Fb + 2 * %G2F + 1 * %G1a +1 * %G1b + 2 * %G2 + 1 * %G1FS(3)1 + 1 * %G1FS(6)1 + 2 * %G2FS(3)1 + 2 * %G2FS(6)1 + 2 * %G2FS(3,3)2 + 2 * %G2FS(3,6)2 + 2 * %G2FS(6,6)2 + 2 * %G2S(6)1 + 2 * %G2S(6,6)2)

Surface plasmon resonance (SPR) analysis

SPR data experiments were performed using a Biacore T100 system (GE Healthcare) and HBS-EP+ (10 mM HEPES, 0,15 M NaCl, 3 mM ethylenediaminetetraacetic acid [EDTA], and 0.05% [v/v] surfactant P20, pH 7.4) as running buffer. Analysis and sample compartment temperatures were set to 25 °C and 4 °C, respectively. The SPR experiments were performed on research-grade CM5 sensor chips. HBS-EP+ (cat# BR100669), Series S Sensor chip CM5 (cat# 29104988) were all from GE Healthcare. Each E5-tagged FcγRs (i.e., FcγRIIIa$_{F158}$, FcγRIIIa$_{V158}$, FcγRIIa, FcγRIIb and FcγRI) was individually captured upon Kcoil previously immobilized at the biosensor surface via coiled-coil interactions as described elsewhere (injections at 0.25 μg/mL) (Cambay et al., 2019). TZM glycoform solutions were injected in triplicate over captured FcγRs and control surfaces at 30 μL/min (FcγRIIIa$_{V158}$) or 50 μL/min (other FcγRs). The receptor/IgG1 dissociation was monitored by injecting running buffer. The surfaces were regenerated with one 20 s injection of 6 M guanidine/HCl at 100 μL/min. Data were collected at a rate of 10 Hz. Prior to analysis, sensorgrams were double-referenced using BiaEvaluation 3.1 software, by subtracting data from the reference flow cell and then subtracting a blank cycle where buffer was injected instead of protein sample. To reduce the influence of spikes in data analysis, 0.5 s of data was removed at injection start and stop. A minimum of one independent replicate for each condition was performed on different days on two different Kcoil surfaces and by two different operators. Representative results are shown.

Cell-based reporter bioassay

Analysis of the binding of the TZM glycoforms to FcγRIIIa was also evaluated using a cell-based reporter bioassay in which engineered Jurkat T-cells expressing either the low-affinity FcγRIIIa$_{F158}$ or the high affinity FcγRIIIa$_{V158}$ variants (Promega, cat# G930A and cat# G701A) were used as effector cells. In addition, these effector cells have also been engineered to express the nuclear factor of activated T-cells (NFAT) signalling cascade linked to luciferase which generates a bioluminescent signal upon engagement of the FcγRIIIa with the Fc portion of an IgG1 interacting with its target expressed on the target cell (i.e. BT-474 cells). Effector cells were propagated in RPMI 1640 (Hyclone, cat#SH30096.01) supplemented with 10% FBS (Hyclone, cat#SH30071.03), 100 μg/mL hygromycin (Invitrogen, cat#10687-010), 250 μg/mL G418 sulfate (Invitrogen, cat#10131-035), 1 mM sodium pyruvate (Gibco, cat#11360-070) and 0.1 mM MEM non-essential amino acids (Gibco cat#11140-050). BT-474 cells which express high levels of HER2 were used as target cells for the TZM glycoforms. The assay was carried out according to the manufacturer's instructions. Briefly, the day prior to the assay, target cells were seeded at 8000 cells per well in the inner 60 wells of 96-well opaque white plates (Corning, cat#3917). Plates were incubated overnight in a humidified incubator at 37 °C with 5% CO_2. Then, TZM glycoforms diluted in the assay buffer (RPMI + 4% low IgG serum (Promega, cat#G7110)) and effector cells were added to wells containing the target cells. After 6 h of incubation (humidified incubator at 37 °C with 5% CO_2), Bioglo luciferase substrate (Promega, cat#G7941) was added to the wells and luciferase activity was quantified by reading the luminescence. Commercial Herceptin and Synagis mAbs were included in the assays as positive and non-specific negative control respectively. The half-maximal effective concentration (EC_{50}) of the TZM glycoforms was calculated in GraphPad Prism (v6.01 for Windows, La Jolla, CA, USA) using a non-linear fit (least squares) with a variable slope.

Statistical analysis

All statistical analyses were performed using GraphPad Prism (v6.01 for Windows, La Jolla, CA, USA). The level of significance was set at $p < 0.05$ using two-tailed tests.

Results

Generation of TZM glycoforms

Production of 6 different TZM glycoforms in CHO cells

The glycoprofile of TZM expressed in CHO cells is essentially composed of fucosylated di-antennary agalactosylated glycan (G0F), and some monogalactosylated glycans (G1F) (Raymond et al., 2015). To obtain distinct TZM glycoforms, the light (LC) and heavy (HC) chains of TZM were co-expressed in CHO cells together with various combinations of enzymes affecting the IgG glycosylation. Culture conditions were similar to those described previously (Raymond et al., 2015). CHO-3E7 cells were transfected with cocktails of plasmids separately encoding TZM LC and HC, human β1,4-galactosyltransferase 1 (β4GT1) and β-galactoside α2,6-sialyltransferase 1 (ST6Gal1) and bacterial GDP-6-deoxy-D-lyxo-4-hexulose reductase (RMD). This enzyme converts the precursor of GDP-fucose into GDP-rhamnose, which in turn inhibits the addition of core fucose on glycans (von Horsten et al., 2010). TZM was either expressed alone (TZM) or co-expressed with β4GT1 (TZM GT),

RMD (TZM RMD), β4GT1 and RMD (TZM GT RMD), β4GT1 and ST6Gal1 (TZM GT ST6), and β4GT1, RMD and ST6Gal1 (TZM GT RMD ST6). The antibodies were then purified on a protein A-column followed by size exclusion chromatography (SEC) to remove aggregates.

Generation of two additional glycoforms by in vitro enzymatic sialylation

Fucosylated and afucosylated disialylated TZM were generated by *in vitro* enzymatic sialylation using TZM GT, TZM GT RMD, TZM GT ST6 and TZM GT RMD ST6 as substrates, in presence of a soluble human ST6Gal1 construct and activated CMP-NANA sugar.

Truncated his-tagged ST6Gal1 devoid of its cytoplasmic and transmembrane domain was expressed by culturing 293-6E cells for 5 day at 37 °C and purified by immobilized metal affinity chromatography (IMAC). Performance of the purification process was evaluated by Coomassie Blue staining of SDS-PAGE performed under non-reducing conditions (Supplementary Fig. S1), which showed almost pure ST6Gal1 with a yield of 22 mg of enzyme/L of culture. Antibodies with disialylated glycans were obtained through an *in vitro* sialylation (IVS) reaction, conducted over 4 day at 37 °C, using TZM glycovariants as substrates for purified ST6Gal1. Reaction mixtures were exchanged every 24 h to eliminate the free CMP resulting from the transfer of sialic acid from CMP-NANA to the protein, after which fresh CMP-NANA was added. Antibodies were then purified on a protein-A column and the efficacy of ST6Gal1 for *in vitro* sialylation was assessed. To this end, fractions were collected every day for lectin blot analysis and the level of sialylation was evaluated using the α2,6-sialylation-specific SNA lectin, while the terminal galactosylation was evaluated using the ECL lectin. The TZM GT IVS, TZM GT ST6 IVS, TZM GT RMD IVS and TZM GT RMD ST6 IVS glycovariants showed increased α2,6-sialylation over time while their terminal galactosylation gradually decreased to undetectable levels (Supplementary Fig. S1), confirming that the soluble ST6Gal1 was active and that the sialylation process was completed.

Characterization of the various TZM glycoforms

Lectin blots

Lectin blots were performed using LCA, ECL, SNA and MALII for the detection of core fucosylation, terminal galactosylation, α2,6-sialylation and α2,3-sialylation respectively (Fig. 1).

The LCA blot showed a strong decrease of the LCA signal for mAbs co-expressed with the RMD enzyme, indicating that the inhibition of the core fucosylation was effective but not complete (Fig. 1a). Co-expression of GT led to an increase in galactosylation level as shown by the strong ECL signals of TZM GT and TZM GT RMD compared to those of TZM and TZM RMD, respectively (Fig. 1b). For the antibodies co-expressed with ST6, the ECL signals were lower than those for TZM GT and TZM GT RMD, suggesting that some but not all galactose residues provided by GT were capped by a sialic acid (Raymond et al., 2015). In contrast, the undetectable ECL signals for the *in vitro* sialylated TZM glycoforms suggests that our sialylation increases the sialylation level in such way that the galactose residues are masked by terminal sialic acid. These results were supported by the SNA signals corresponding to the antibodies co-expressed with ST6 and *in vitro* sialylated with ST6Gal1 (Fig. 1c). Moreover, the SNA signals were higher for the *in vitro* sialylated TZM glycoforms compared to antibodies co-expressed with ST6. Noteworthy, the signals were weaker for antibodies co-expressed with RMD. Finally, the MALII blot indicated that none of the antibody samples contained detectable amounts of α2,3 sialic acids (Fig. 1d). We thus concluded that the presence of α2,3-sialylation was not significant.

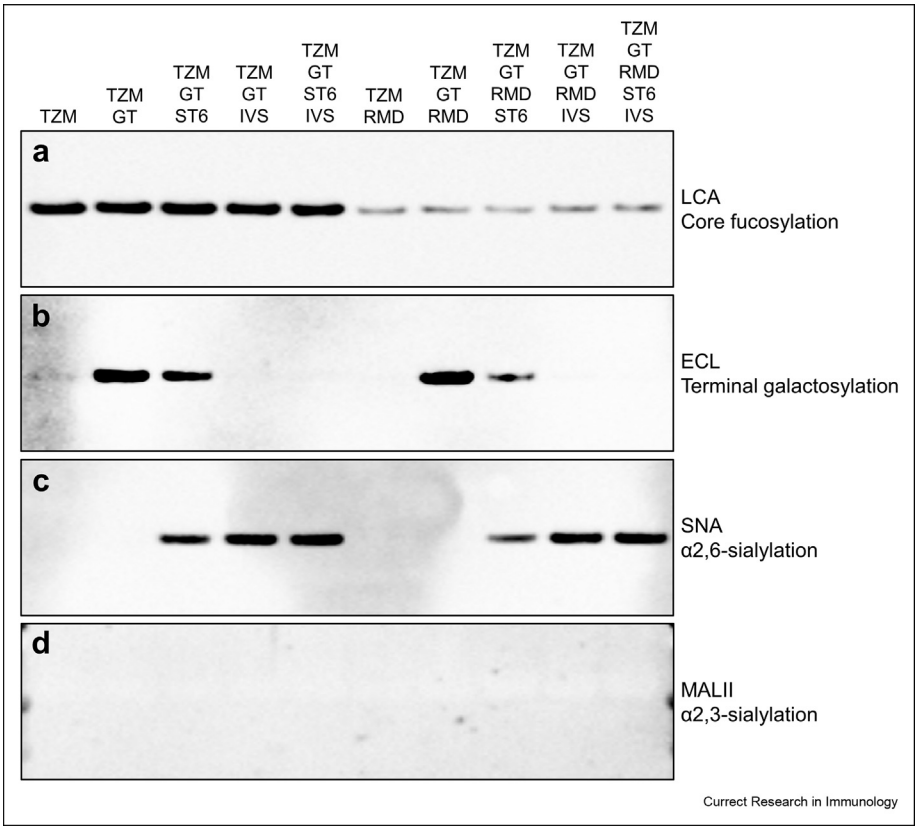

Fig. 1. Lectin blot analysis of the ten TZM glycoforms. The lectin blots were performed with purified TZM under reducing conditions. Only the bands corresponding to the heavy chains of the antibodies are shown. LCA (**a**), ECL (**b**), SNA (**c**) and MALII (**d**) were used to detect core fucosylation, terminal galactosylation, α2,6-sialylation and α2,3-sialylation respectively.

Capillary isoelectric focusing

The charge profile of the mAbs was analysed by cIEF. TZM was shown to be composed of two main variants (≈91.5%) flanked by three minor variants (Fig. 2a). TZM had a profile similar to that of non-glycosylated TZM (data not shown) and antibodies that were produced without ST6 (i.e. TZM GT, TZM RMD, and TZM GT RMD; these IgG1s will be designated as the "neutral mAbs" from this point on) (Fig. 2b–d). In contrast, the charge variant profiles of the antibodies co-expressed with ST6 (TZM GT ST6 and TZM GT RMD ST6) were drastically different (Fig. 2e and f). Peaks corresponding to variants #2 and #3 (see Fig. 2a) dropped to ≈52–54.5%, while acidic variants were more abundant, especially variants #4 and #5 (representing ≈ 27.5–29.5%) and #6, #7, #8 (≈17%). Lastly, profiles were most different for the *in vitro* sialylated antibodies, for which variants #2 and #3 dropped to ≈ 5–13.5% (Fig. 2g–j), while the acidic variants sharply increased with variants #4 and #5 representing ≈11.5–17% and the remaining acidic variants representing ≈65–79.5%. The increase of acidic variants for the TZM co-expressed with ST6 as well as *in vitro* α2,6-sialylated TZM also correlated to the decrease of the calculated apparent isoelectric points (pIs). Altogether, the cIEF profiles of the TZM variants are in agreement with the lectin blots since the increase of acidic variants can be attributed to a higher content in sialic acid (Raymond et al., 2012).

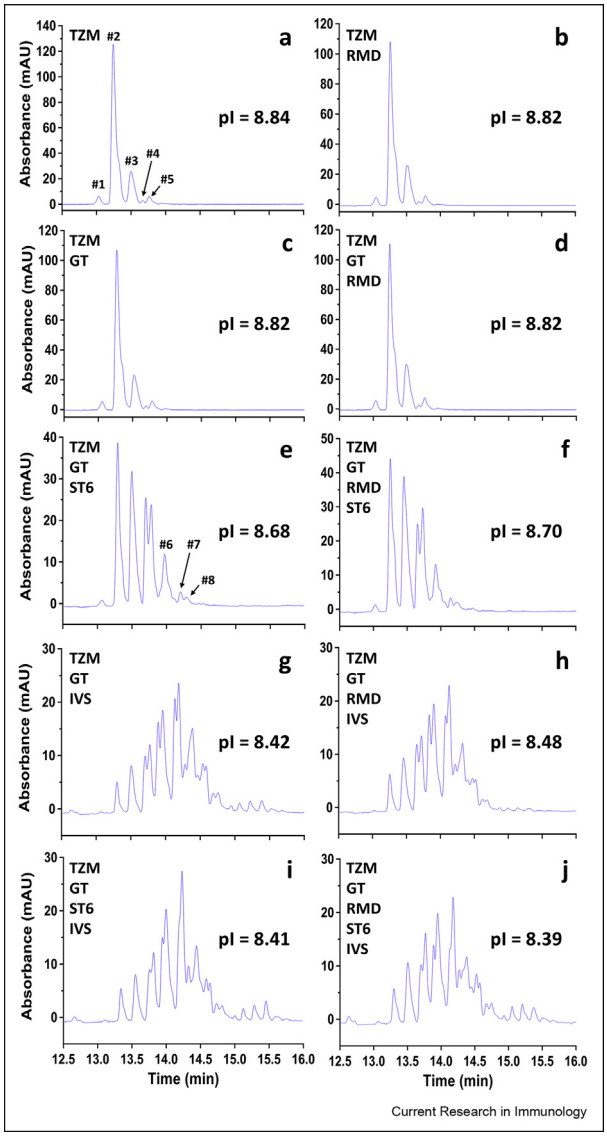

Fig. 2. cIEF profiles of the ten TZM glycoforms. (**a-j**) cIEF profiles of purified TZM alone or co-expressed with GT, ST6 and/or RMD as well as *in vitro* α2,6-sialylated. Calculated apparent pIs of the ten TZM glycoforms are also shown.

Hydrophilic interaction liquid chromatography

The characterization of the TZM glycoforms was complemented by a HILIC analysis of the glycans released by a PNGaseF treatment (Fig. 3). N-glycans were identified through database comparison and confirmed by exoglycosidase digestion (Raymond et al., 2015). Seventeen different N-glycans were identified across the ten mAbs analysed and all were of the complex di-antennary type. The abundance of each species was calculated according to the area under the corresponding peak. Each antibody was analysed in duplicate and the averages of the quantification are presented in Table 1. The unidentified glycans (u.g.) represented a maximum of 7% of the peak areas, excepted for TZM GT RMD IVS and TZM GT RMD ST6 IVS for which unidentified glycans represented 15.1% and 17%, respectively.

TZM exhibited the typical profile expected from an IgG1 expressed in CHO cells (Fig. 3) (Raymond et al., 2015). The glycoprofile comprised mainly G0F (66.9%), the two G1F isomers (19% and 6.2%) and very low amounts of G2F (3%) (Table 1). Few afucosylated glycans G0 and G1 were detected (1% and 0.8% respectively), as well as very low amounts of α2,3-sialylated species (0.6%).

The co-expression of TZM with GT (TZM GT) showed an increased level of fully galactosylated glycan G2F (55.6%) and a small increase in the level of mono-α2,3-sialylated glycan (13%) (Table 1).

The co-expression of TZM with RMD (TZM RMD) resulted in a substantial decrease of fucosylation (from >98% to 15%). This decrease was less pronounced when RMD was co-expressed with GT or GT and ST6 (Table 1): 37% and 33% of the glycans remained fucosylated in TZM GT RMD and TZM GT RMD ST6, respectively. In addition, TZM RMD contained less than 1% fucosylated digalactosylated glycans (G2F, G2FS1, G2FS2). These forms represented as much as 24% and 26.5% in TZM GT RMD and TZM GT RMD ST6, respectively. Also, less than 4% of sialylated glycans were detected in TZM GT RMD as compared to 10% in TZM GT (Fig. 4).

ST6 co-expression led to the production of α2,6-sialylated glycans (Table 1); α2,6-sialic acid represented 81%–97% of all sialic acids. In agreement with our lectin blot analysis, TZM GT ST6 showed a higher α2,6-sialylation level than TZM GT RMD ST6 (33% and 25% of sialylated glycans, respectively). The most abundant sialylated glycan was mono-α2,6-sialylated G2FS(6)1 in TZM GT ST6 (32% of the glycans), and its afucosylated counterpart G2S(6)1 in TZM GT RMD ST6 (16.6%). However, G2FS(6)1 levels were relatively high in TZM GT RMD ST6 (14.4%). Interestingly, we found that in TZM GT RMD ST6, 69% of the fucosylated digalactosylated species were sialylated, whereas only 38% of the non fucosylated digalactosylated glycans were (Table 1).

Finally, the *in vitro* sialylation of TZM GT IVS, TZM GT ST6 IVS, TZM GT RMD IVS and TZM GT RMD ST6 IVS resulted in a α2,6-sialylated glycan content of 74%, 75.5%, 60% and 69%, respectively. This was accompanied by a decrease of the proportion of glycans with terminal galactose units (Fig. 4). The level of G2FS(6,6)2 was increased to 40.6% (TZM GT IVS) and 43.8% (TZM GT ST6 IVS), while a non-negligible level of G2FS(6)1 remained (19.7% and 18.6% for TZM GT IVS and TZM GT ST6 IVS, respectively, see Table 1). For TZM GT RMD IVS and TZM GT RMD ST6 IVS, the percentage of glycoforms being both afucosylated and di-α2,6-sialylated were only 20.1% and 26%, respectively. Indeed, we found that some α2,6-sialylated glycans were still fucosylated and only 58% and 64% of α2,6-sialylated glycoforms were afucosylated with the TZM GT RMD IVS and TZM GT RMD ST6 IVS samples, respectively. We also showed that regardless of the substrate (co-expression with GT in absence or presence of ST6), similar levels of di-α2,6-sialylation were reached. Therefore, it was concluded that, a monosialylated substrate does not lead to increased disialylation and, given that the majority of galactoses were capped with sialic acid, the disialylation process was more likely limited by the initial levels of digalactosylated species.

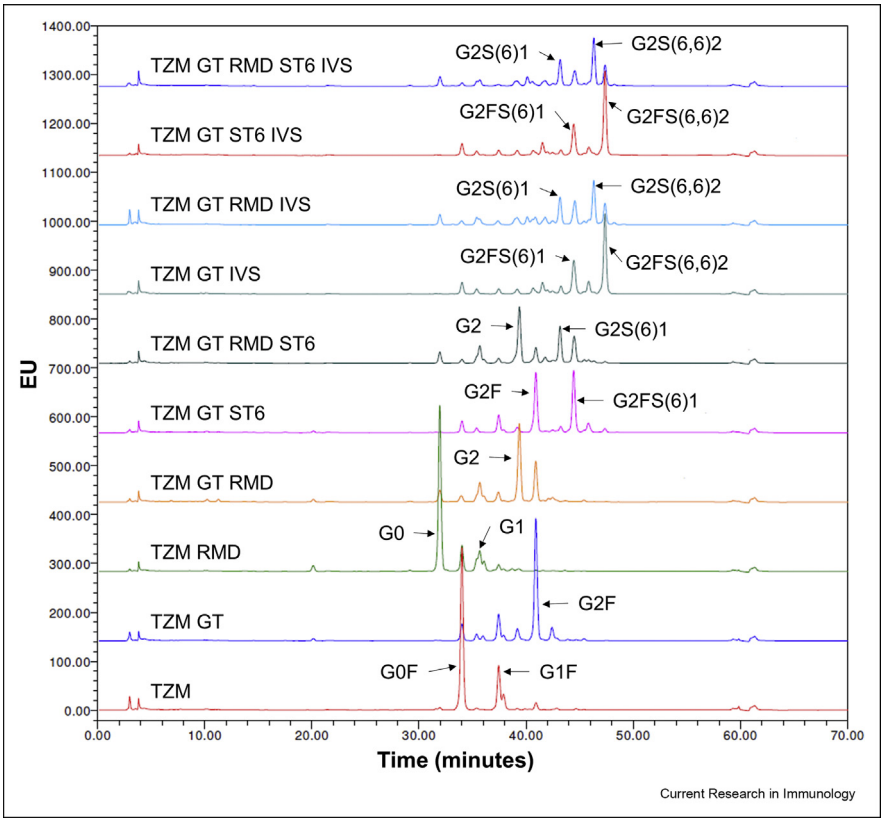

Fig. 3. HILIC analysis of PNGaseF-released glycans for the ten TZM glycoforms. Identification was performed by database comparison and confirmed by exo-glycosidase digestion. The schematic representation of the N-glycans nomenclature is presented in Table 1.

Evaluation of the interactions with the FcγRs by SPR

Determination of the thermodynamic dissociation constants (K_D)

The impact of the glycosylation pattern of TZM on its binding to the FcγRs was evaluated by an SPR assay we recently developed (Cambay et al., 2019). The assay relies on the stable and oriented capture of the distinct FcγRs through the interaction of the E5 peptide with which the FcγRs are tagged with its K5 peptide partner bound to the biosensor surface, followed by the injection of the TZM glycoforms. E5-tagged low-affinity FcγRs (i.e., $FcγRIIIa_{F158/V158}$ and FcγRIIa/b) were produced in CHO and HEK293 cell lines to determine the impact of FcγR N-glycan profiles upon binding of the various TZM preparations. In contrast, the E5-tagged high-affinity FcγRI was produced only in CHO cells, due to very low expression level obtained in HEK293 cells. Fig. 5 shows several representative control-corrected SPR sensorgrams depicting the interaction of fucosylated or afucosylated TZM with the various FcγRs.

For the low-affinity FcγRs, the apparent K_D values were calculated through a steady-state analysis assuming a one-to-one binding model. In the case of FcγRI, plateaus were not reached at the end of the TZM injections, and data were therefore globally fit in order to determine the apparent kinetic constants (k_a and k_d) and to deduce the apparent K_D values ($K_D = k_d/k_a$) of these interactions. A kinetic model corresponding to the existence of two distinct populations of captured FcγRI was also applied to analyse the data since i) a simpler kinetic model gave poor fit and ii) traces of receptor aggregates were observed in our receptor preparation by analytical SEC (Supplementary Fig. S2). The apparent K_D values for each receptor/TZM glycoform interaction are presented in Fig. 6 and the Supplementary Table S1 (note two distinct K_D values are reported here; K_D1 and K_D2 each corresponding to the monomeric and aggregated FcγRI populations, respectively, for this specific receptor).

In agreement with the literature, apparent K_Ds varied the most with the FcγR type, with TZM apparent K_D values within the 10^{-6} – 10^{-7} M range for the low-affinity FcγRs and in the 10^{-9} M range for the FcγRI (Bruhns et al., 2009; Lu et al., 2015), whereas in case of FcγRIIIa, the apparent K_D values of afucosylated TZMs were reported to be in the 10^{-7} – 10^{-8} M range (Zeck et al., 2011; Subedi and Barb, 2016). Here we report that affinities of the IgG1 fucosylated forms for the FcγRs could be ranked as follows: FcγRI » $FcγRIIIa_{V158}$ > FcγRIIa > $FcγRIIIa_{F158}$ > FcγRIIb. Affinities for the afucosylated forms ranked as: FcγRI > $FcγRIIIa_{V158}$ > $FcγRIIIa_{F158}$ » FcγRIIa > FcγRIIb.

IgG1-Fc N-glycan sugar moieties influence upon FcγRs binding

The IgG1-FcγRs interaction is also influenced by the IgG1-Fc N-glycan profile for a given receptor. Indeed, besides the major and well-documented changes in affinity observed for the IgG1 interactions with $FcγRIIIa_{F158/V158}$ (>2-fold) (Dekkers et al., 2017; Subedi and Barb, 2016), our enhanced SPR-based assay also allowed to highlight minor (<2-fold) but significant effects of IgG1-Fc N-glycan variation upon FcγRIIa and FcγRI binding. The influence of IgG1 fucosylation on FcγR binding is shown in Fig. 6a–e while the influence of IgG1 N-glycan galactosylation, monosialylation or disialylation is displayed in Fig. 6f–j.

In agreement with the literature, Fig. 6a and b shows that the absence of core fucose within the IgG1 N-glycan led to the most significant ($p \leq 0.0001$) increase of affinity for TZM binding to both FcγRIIIa variants (18–32-fold increase depending on the FcγRIIIa variant and the level of IgG1 N-glycan afucosylation) (Dekkers et al., 2017; Shields et al., 2002; Subedi and Barb, 2016). In addition, as shown by Subedi et al. (Subedi and Barb, 2016), no significant effect was observed for FcγRIIa, FcγRIIb and FcγRI binding (Fig. 6c, d and 6e respectively).

Dekkers et al. (2017) have shown that the addition of two galactose residues led to a 2-fold increase of the affinity of afucosylated IgG1s for both FcγRIIIa variants and Subedi et al. (Subedi and Barb, 2016) have reported an average 1.7-fold increase in affinity for all FcγRs except

Table 1
Relative abundance of the glycans detected in the HILIC chromatograms.

GU	Glycans	Schematic representation	TZM	TZM GT	TZM GT ST6	TZM GT IVS	TZM GT ST6 IVS	TZM RMD	TZM GT RMD	TZM GT RMD ST6	TZM GT RMD IVS	TZM GT RMD ST6 IVS
5.91	G0F		**66.9**	7.5	5.6	5.8	6.0	**10.2**	3.7	1.8	2.1	1.7
6.66	G1Fa (pr. G(6)1F)		**19.0**	**11.9**	8.5	2.9	2.9	2.6	5.5	2.5	2.1	1.1
6.76	G1Fb (pr. G(3)1F)		6.2	2.2	1.2	0	0	0.8	0.7	0.4	0.1	0.1
7.49	G2F		3.0	**55.6**	**31.5**	0	1.0	0.3	**20.5**	8.3	3.7	0
5.49	G0		1.0	0.2	0.1	0.1	0.1	**64.8**	5.6	4.8	4.6	4.9
6.27	G1a (pr. G(6)1)		0.7	3.0	2.3	2.6	2.2	**12.4**	**12.0**	**10.1**	5.9	5.3
6.34	G1b (pr. G(3)1)		0.1	2.1	0.2	0.2	0.3	3.8	2.6	1.3	0	0
7.08	G2		0	0	0	0	0	1.2	**39.5**	**28.5**	5.8	4.8
7.08	G1FS(3)1		0.4	6.5	3.4	2.8	2.9	0	0	0	0	0
7.66	G1FS(6)1		0	0.6	0	6.0	6.8	0.2	0.9	0	0	0
7.92	G2FS(3)1		0.2	6.6	1.5	1.7	1.6	0.1	3.0	1.7	2.2	1.6
8.51	G2FS(6)1		0.6	0.6	**31.7**	**19.7**	**18.6**	0.3	0.3	**14.4**	**13.4**	**10.9**
8.4	G2FS(3,3)2		0	0.2	0	0	0	0	0.1	0	0	0
8.91	G2FS(3,6)2		0	0	5.4	6.2	4.7	0	0	1.5	2.0	1.8
9.42	G2FS(6,6)2		0	0	2.1	**40.6**	**43.8**	0	0	0.7	**10.1**	**11.3**
8.12	G2S(6)1		0	0	3.1	3.9	3.1	0	0	**16.6**	**13.4**	**14.6**
9.06	G2S(6,6)2		0	0	0	0.7	0.8	0	0.1	1.1	**20.1**	**26.0**
7.72	u.g.		0.1	0	1.1	0	0	0	0	3.6	4.9	4.7
	u.g. other		2.2	3.7	2.4	6.9	5.8	3.5	6.4	2.9	10.2	12.3

The relative glycan abundance was calculated as the area under the peak attributed to the glycan, divided by the sum of the areas of all the peaks detected in the chromatogram. N-glycans were attributed to the peaks detected by comparison of the peaks glucose units (GU) values to database. The values in bold correspond to abundances ≥10%. The symbolic representation of the sugars is: N-acetylglucosamine (blue square), mannose (green circle), galactose (yellow circle), N-acetylneuraminic acid (α2,6) (pink diamond), N-acetylneuraminic acid (α2,3) (blue diamond) and fucose (red triangle). pr.: presumably, u.g.: undetermined glycan.

FcγRI. We report here, that the addition of two galactose also led to such increase of affinity between IgG1s (regardless of the level of IgG1 fucosylation) and all FcγRs (Fig. 6, right panels). More specifically, the FcγRIIIa$_{F158/V158}$ binding was the most affected (2-fold increase; Fig. 6f and g) and to a lesser extent the FcγRIIa/b binding (1.2-fold increase; Fig. 6h and i). Surprisingly, a statistically significant ($p \leq 0.01$) impact of the IgG1 N-glycan galactosylation on FcγRI binding was also observed (1.4-fold increase in affinity; Fig. 6j).

For all FcγRs, higher mono- and di-α2,6-sialylation levels of the IgG1s led to an increase in affinity similar to that of digalactosylation (when compared to the G0F or G0 forms). However, while a low level of mono-α2,6-sialylation (GTST6 and GTRMDST6) upon digalactosylation did not seem to improve the IgG1 affinity, higher mono- and di-α2,6-sialylation levels (GTIVS, GTST6IVS, GTRMDIVS and GTRMDST6IVS) negatively impacted the IgG1 affinity compared to the digalactosylated IgG1s. Of interest, only the FcγRI binding was not negatively affected by high levels of sialylation. These results for FcγRIIa/b have also been observed by Dekkers et al. (2017) but are contrasted with those observations reported on by Subedi et al. (Subedi and Barb, 2016).

Lastly, the TZM N-glycan variations similarly affected FcγRs binding, regardless of the FcγRs expression system used. The only difference observed, as reported previously (Hayes et al., 2017; Cambay et al., 2019), was for both FcγRIIIa variants, with higher affinities recorded for HEK293-produced receptor proteins.

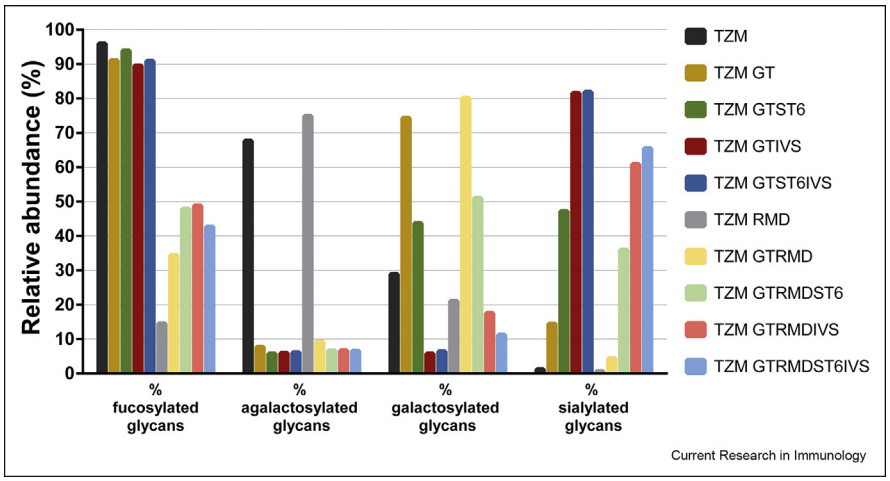

Fig. 4. Relative abundance of glycan families (fucosylated, agalactosylated, galactosylated and sialylated glycans).

In vitro cell-based bioassay

The impact of the TZM N-glycan pattern on TZM interaction with $Fc\gamma RIIIa_{F158/V158}$ was also evaluated *in vitro* using a reporter bioassay. In this assay, Jurkat cells expressing either the low-affinity F158 variant or the high-affinity V158 variant of the FcγRIIIa transduce, upon IgG1 binding, intracellular signals resulting in NFAT-mediated luciferase activity. Briefly, TZM glycoforms were first incubated with the target cells (BT-474 cells expressing high levels of HER2), after which the engineered Jurkat effector cells were added. Commercial Herceptin was included in the assays as a positive control while Synagis (palivizumab, an anti-Respiratory Syncytial Virus Fusion glycoprotein [RSVF] antibody) and non-glycosylated TZM were included as negative controls (Fig. 7).

Recent studies from other groups investigated the impact of IgG1 Fc N-glycan upon ADCC activity and all observed an increase for afucosylated IgG1 forms (Dekkers et al., 2017; Wada et al., 2019; Li et al., 2017). In addition, terminal galactosylation was also reported to increase, while di-α2,6-sialylation slightly decreased the ADCC activity. However, the negative impact of sialylation was observed either for afucosylated IgG1s (Dekkers et al., 2017), fucosylated IgG1s (Li et al., 2017) or both (Wada et al., 2019).

When comparing the bioassay response of highly-fucosylated TZMs to low-fucose variants, we observed an increase in bioluminescent signal (Fig. 7a: 4- to 12-fold for the $Fc\gamma RIIIa_{F158}$ variant; Fig. 7b: 1.5–4.5-fold for its V158 counterpart). Furthermore, calculating the EC_{50} showed a decrease of ~2.5-fold for the F158 variant and a ~2.5- to 4-fold for V158 variant (Supplementary Table S2). The lowest EC_{50} for the F158 and V158 variants were observed for the TZM GT RMD ST6 (14.71 ng/mL) and TZM GT RMD (6.79 ng/mL), respectively (Supplementary Table S2, Fig. 7c and d). These results imply that the absence of core fucose in an IgG1 also has a major effect in terms of triggering a cellular response.

The impact of the IgG1-Fc N-glycan elongation was similar for both FcγRIIIa variants (Fig. 7c and d). Indeed, regardless of the fucosylation level, the strongest responses were recorded for the glycoforms carrying terminal galactosylation or terminal α2,6-sialylation, with slight differences between them. In contrast, the signals corresponding to the low-galactosylated glycoforms (TZM and TZM RMD) were lower. More precisely, according to the EC_{50}, besides the absence of fucose, the most pronounced positive influence was observed for the digalactosylated glycoforms in our cell assay. In terms of sialylation, a small increase in monosialylation level had no impact. Lastly, higher level of sialylation negatively affected the cellular assay response for both fucosylated and afucosylated forms.

Altogether, the relative *in vitro* cell assay response of high- and low-fucosylated TZM glycoforms as well as the subtle differences between agalactosylated, galactosylated and sialylated glycoforms were consistent with the apparent K_D values determined in our enhanced SPR-based assay (Fig. 7e and f).

Discussion

Over the last two decades, many studies have evaluated the effect of IgG1 glycosylation on their effector functions (ADCC or CDC). More specifically, most of these studies have focused on terminal galactosylation, terminal sialylation and/or the absence of core fucose (Dekkers et al., 2017; Shields et al., 2002; Thomann et al., 2015; Wada et al., 2019; Subedi and Barb, 2016; Dashivets et al., 2015; Li et al., 2017; Scallon et al., 2007; Kurogochi et al., 2015; Lin et al., 2015; Houde et al., 2010). While there is a consensus on the positive effect of IgG1-Fc afucosylation for FcγRIIIa binding (and in turn on ADCC activity), the influence of both terminal galactosylation and terminal α2,6-sialylation remains ambiguous. Discrepancies found in the literature can be partly attributed to the differences in experimental procedures used to prepare and enrich specific IgG1 glycovariants. As such several methodologies, including chemoenzymatic glycoengineering (Wada et al., 2019; Li et al., 2017; Shivatare et al., 2018; Lin et al., 2015; Tsukimura et al., 2017) and *in vitro* glycoengineering (Yamaguchi et al., 2006; Thomann et al., 2015; Dashivets et al., 2015; Peschke et al., 2017; Yu et al., 2013), combined or not with the transient co-expression (Dekkers et al., 2016) or the inhibition of enzymes involved in the N-glycosylation process (Subedi and Barb, 2016), have been used and may have resulted in differences in terms of homogeneity for these IgG1 lots. Altogether, only a few studies investigated a complete panel of IgG1 glycoforms to provide a holistic comprehensive overview of the influence of IgG1 glycosylation on immune cell effector functions (Dekkers et al., 2017; Wada et al., 2019; Subedi and Barb, 2016). Thus, there is still a need to strengthen these observations in an independent fashion and evaluate how they translate to another antibody.

Using Trastuzumab as our parent IgG1 we thus generated eight glycovariants using a mammalian expression method that mainly relies on the over-expression of enzymes involved in the N-glycosylation pathway. More specifically, six IgG1 glycoforms were produced by transient co-

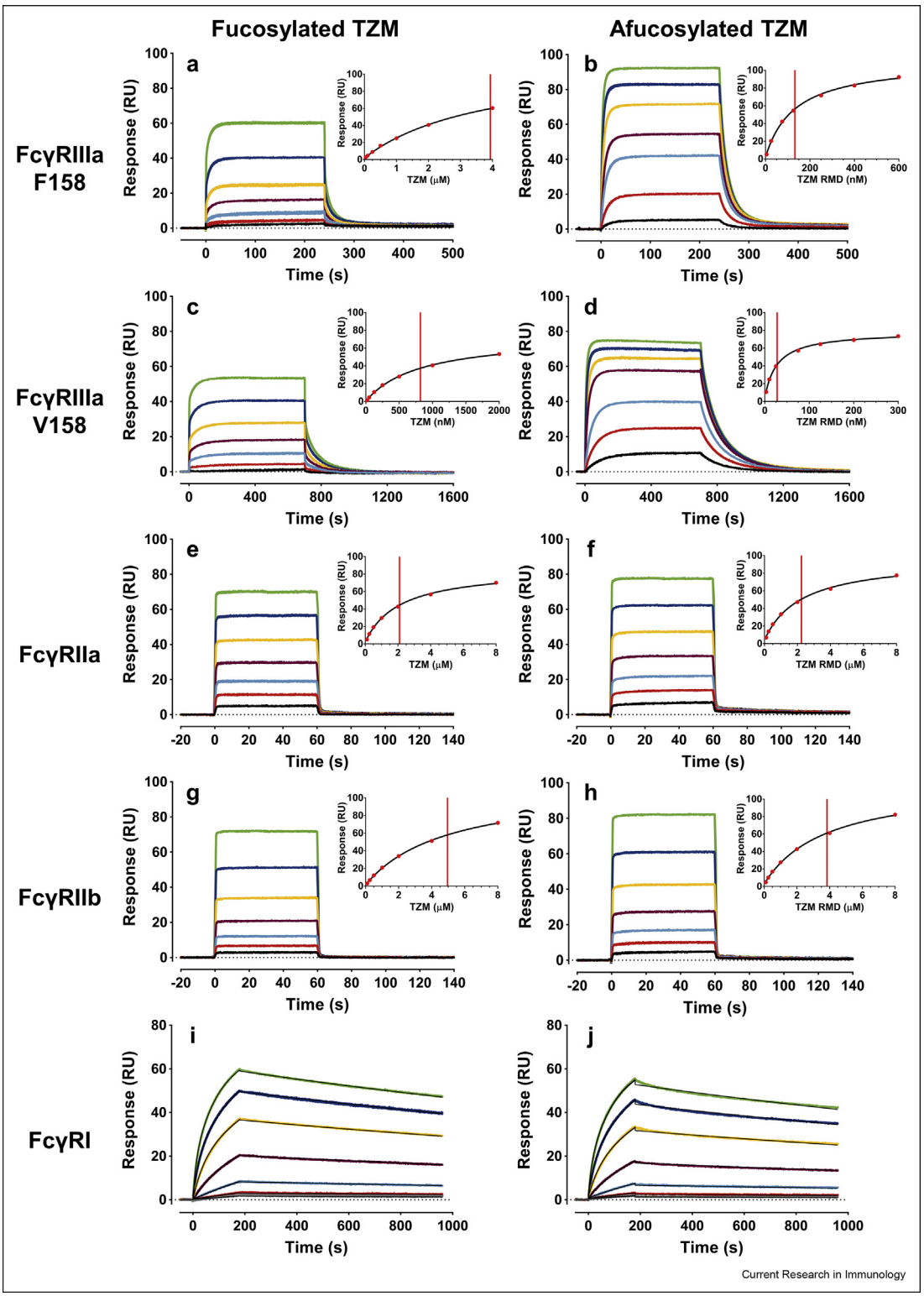

Fig. 5. Representative control-corrected SPR sensorgrams corresponding to the interactions of various TZM glycoforms with captured FcγRs. Sensorgrams corresponding to the interactions of fucosylated TZM (left column, TZM) or afucosylated TZM (right column, TZM RMD) with E5-tagged FcγRs previously captured on a K5 surface (≈30 RUs of FcγRIIIa$_{F158}$ (**a,b**); ≈20 RUs of FcγRIIIa$_{V158}$ (**c,d**); ≈20 RUs of FcγRIIa (**e,f**); ≈25 RUs of FcγRIIb (**g,h**) and ≈45 RUs of FcγRI (**i,j**)). Each data set corresponds to the triplicate injection of a TZM glycoform at 7 concentrations (between 40-4000 nM for fucosylated TZM-FcγRIIIa$_{F158}$; 5–600 nM for afucosylated TZM-FcγRIIIa$_{F158}$; 20-2000 nM for fucosylated TZM-FcγRIIIa$_{V158}$; 3–300 nM for afucosylated TZM-FcγRIIIa$_{V158}$; 100-8000 nM for FcγRIIa and FcγRIIb; 0.5–100 nM for FcγRI). (**a-h**) The steady state analysis of the sensorgrams is shown in the insets with the vertical line marking the respective calculated K_D values. (**i, j**) The thin black solid lines correspond to the global fit using a kinetic model assuming the existence of two distinct populations of captured FcγRI.

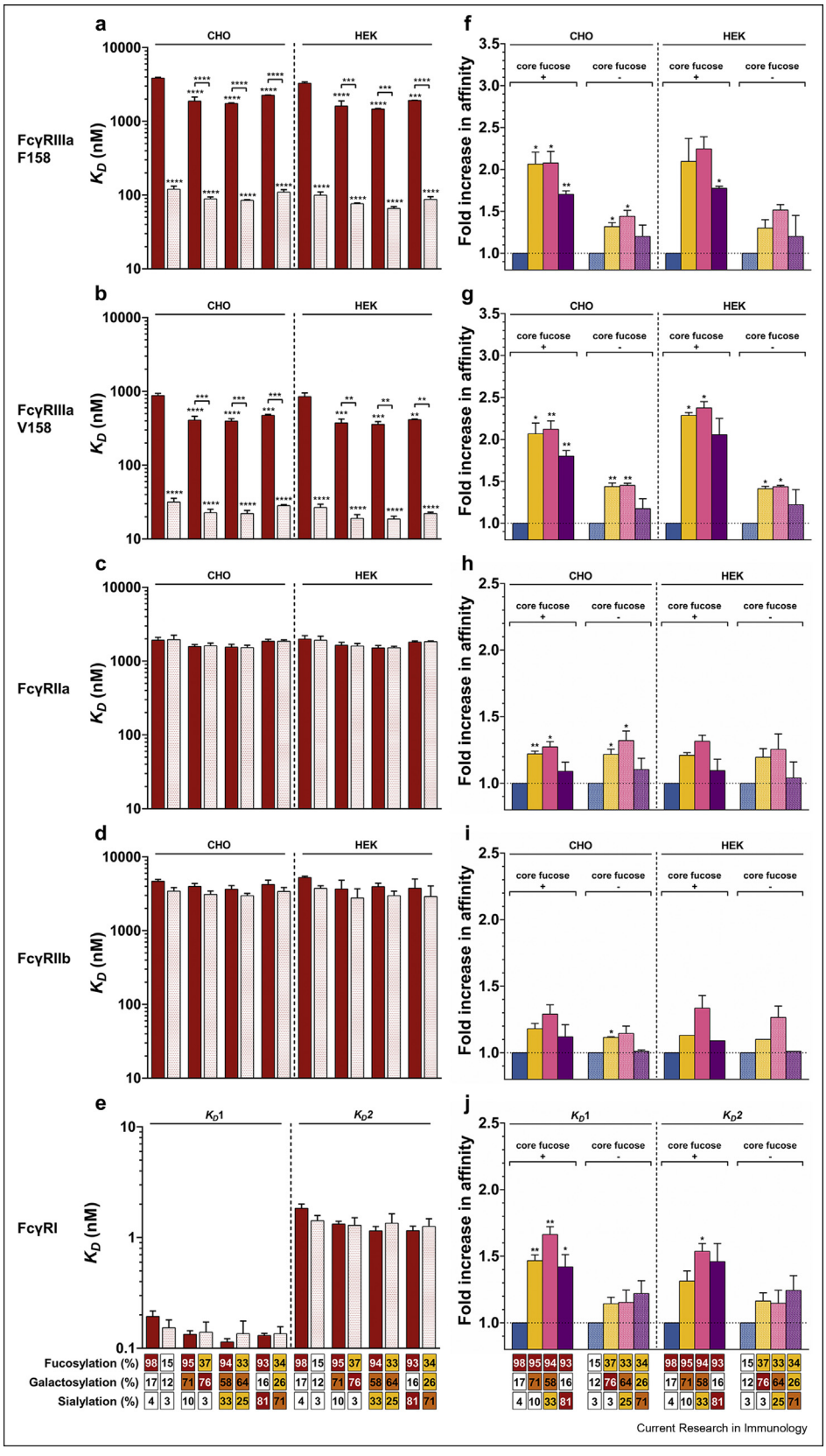

Fig. 6. Influence of the IgG-Fc N-glycan sugar moieties upon FcγR binding. (**a-e**) The impact of Fc core fucosylation on FcγR binding affinity. K_D values are representative of at least 2 independent experiments for each condition and the standard errors of the mean (SEM) are shown. **, *** and **** denote a statistical significance of $p \leq 0.01$, $p \leq 0.001$, and $p \leq 0.0001$, respectively, as tested by one-way ANOVA using Tukey's multiple comparisons test against TZM, or comparing the fucosylated vs afucosylated forms with the same N-glycan elongation level as indicated by the horizontal lines). (**f-j**) The impact of terminal sugar moieties (i.e., digalactosylation, mono-α2,6-sialylation and di-α2,6-sialylation) of the IgG1-Fc N-glycan on FcγRs binding relative to TZM (filled column) or TZM RMD (hatched column). The ratios are representative of at least 2 independent experiments and SEM are shown. * and ** denote a statistical significance of $p \leq 0.05$ and $p \leq 0.01$, respectively, as tested by a one-sample *t*-test against a theoretical mean of 1. The abscissa legend describes the percentage of each glycan family.

expression of the β1,4-galactosyltransferase 1 (GT) and/or the β-galactoside α2,6-sialyltransferase 1 (ST6), and/or the GDP-4-dehydro-6-deoxy-D-mannose reductase (RMD). This resulted in TZM glycovariants with increased levels of terminal galactosylation and terminal α2,6-sialylation, and reduced fucosylation, respectively. In our hands, transient co-expression of TZM with several enzymes (i.e., GT with ST6 or GT with RMD and ST6) led to higher N-glycan heterogeneity when compared to that reported with strategies relying on chemoenzymatic

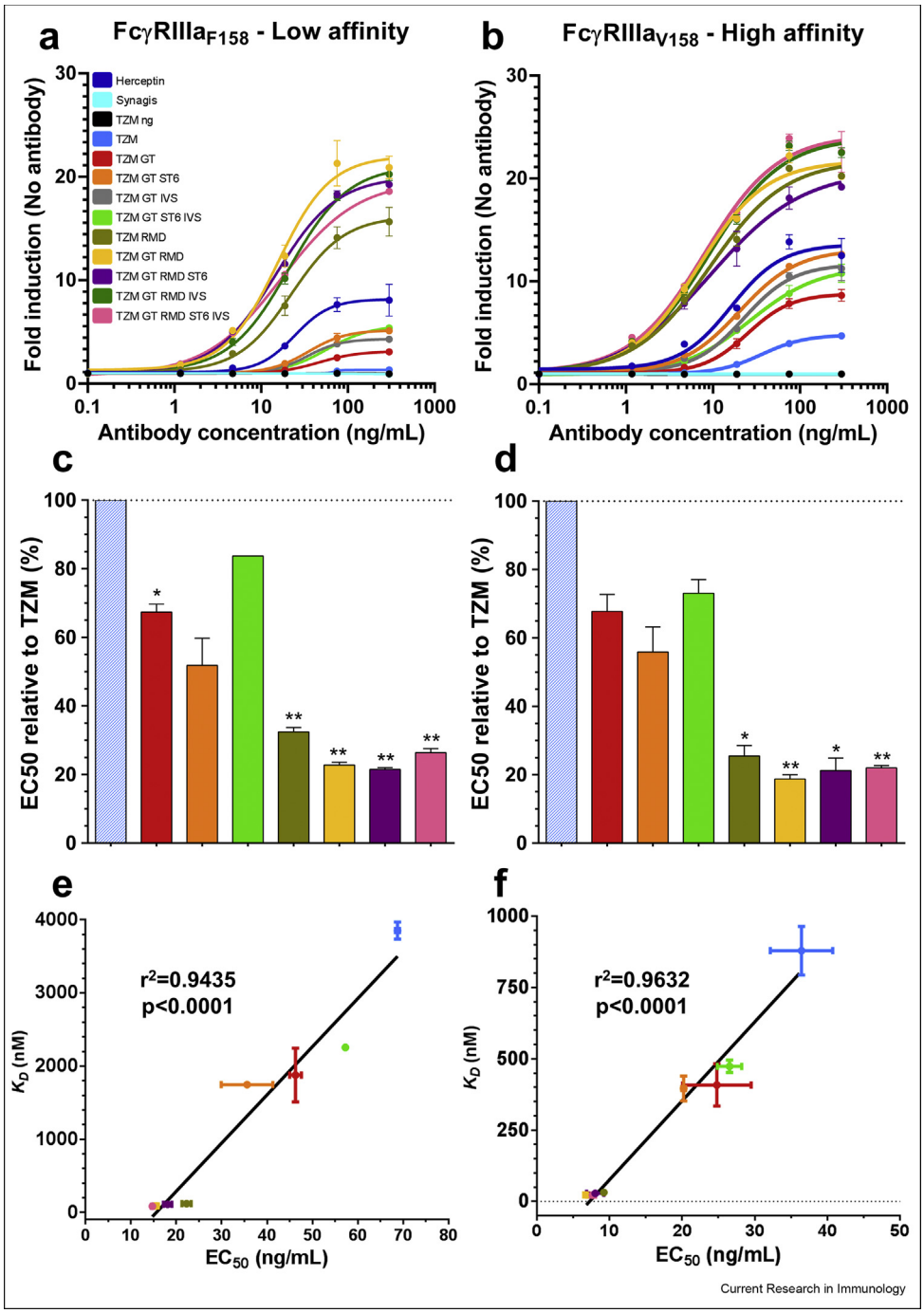

Fig. 7. Reporter assay responses induced by the TZM glycoforms. The antibodies were put in contact with target cells expressing HER2 and effector cells expressing the low affinity FcγRIIIa$_{F158}$ (**a**) or the high affinity FcγRIIIa$_{V158}$ (**b**). The response was measured as a bioluminescent signal produced by the effector cells upon antibody binding, and expressed as a multiple of the basal bioluminescent signal produced by the effector cells in absence of antibodies. The results are the average and standard deviations of duplicates. Commercial Herceptin was included in the assays as positive control while Synagis and non-glycosylated TZM (TZM ng) were included as negative controls. The half maximal effective concentration (EC$_{50}$) for each TZM glycoforms was calculated using a non-linear fit (least squares) with a variable slope and displayed as relative EC$_{50}$ compared to TZM (hatched columns) for the FcγRIIIa$_{F158}$ (**c**) and FcγRIIIa$_{V158}$ (**d**). The data represent the mean and SD; * and ** denote a statistical significance of $p \leq 0.05$ and $p \leq 0.01$, respectively, as tested by a one-sample *t*-test against a theoretical mean of 100 (%). Correlation between apparent K_D values of FcγRIIIa$_{F158}$ (**e**) or FcγRIIIa$_{V158}$ (**f**) binding of TZM glycoforms and EC$_{50}$. r^2 and p value of the linear regression are shown.

glycoengineering (Wada et al., 2019; Li et al., 2017; Tsukimura et al., 2017). Enzyme co-expression caused only partial inhibition of fucosylation while the levels of α2,6-sialylated glycoforms, although increased, mostly corresponded to the mono-α2,6-sialylated digalactosylated species, which is in agreement with previous observations (Raymond et al., 2015; Dekkers et al., 2016). Taking into account glycoform heterogeneity (in order to better interpret our results from our SPR assay), a complete characterization of our glycoforms was thus performed using three orthogonal methods (Figs. 1–3; Table 1), which all led to the same conclusions in respect to the major differences observed from one TZM glycoform preparation to the other (Fig. 4).

To complete our TZM glycoform panel and to determine the impact of higher di-α2,6-sialylation levels, *in vitro* α2,6-sialylation of TZM expressed in presence of GT only, GT/RMD, GT/ST6 and GT/RMD/ST6 was performed with a soluble ST6Gal1 construct. In accordance with the literature, this resulted in the enrichment of a di-α2,6-sialylated IgG1 although the amount of mono-α2,6-sialylated species remained substantial, suggesting that the limited disialylation was more probably due to incomplete IgG1 digalactosylation (Dekkers et al., 2016).

Altogether, our results have shown that, compared to cell line engineering and complete *in vitro* glycoengineering, transient co-expression of three enzymes associated with only one additional *in vitro* α2,6-sialylation step led to the rapid generation (within two weeks) of eight distinct and well-defined TZM glycoforms at high yields and at reasonable costs. Nonetheless, transient co-expression has shown some limitations and led to higher N-glycan heterogeneity compared to

chemoenzymatic glycoengineering.

There is no consensus on the effect of IgG1-Fc N-glycan content on FcγRs binding in the literature. Several methods have been used to characterize these interactions, including affinity chromatography (Thomann et al., 2015; Wada et al., 2019; Dashivets et al., 2015), ELISA (Li et al., 2017; Shivatare et al., 2018; Kurogochi et al., 2015; Lin et al., 2015) and SPR analysis (Dekkers et al., 2017; Thomann et al., 2015; Wada et al., 2019; Subedi and Barb, 2016; Dashivets et al., 2015; Li et al., 2017), applied in many variations, which in turn led to major differences in the interpretation of the results (Cambay et al., 2019). In addition, the interactions were assessed either for all FcγRs (Dekkers et al., 2017; Subedi and Barb, 2016; Lin et al., 2015; Bruggeman et al., 2017) or only for FcγRIIIa (Wada et al., 2019; Li et al., 2017; Peschke et al., 2017; Kurogochi et al., 2015; Houde et al., 2010) as FcγRIIIa binding (and consequently the ADCC activity) has been reported to be the most affected by the IgG1 N-glycan profile.

In the study reported here, we recorded the binding kinetics of eight TZM glycoforms to a panel of human FcγRs (i.e., FcγRIIIa$_{F158}$, FcγRIIIa$_{V158}$, FcγRIIa, FcγRIIb and FcγRI) using a SPR assay (Fig. 5) that outperformed in our hands other capture approaches relying on his-tagged or biotinylated receptors in terms of reproducibility (Cambay et al., 2019). The TZM glycovariants/FcγRs binding was further analysed with FcγRs produced either in CHO or HEK293 cell line. Some studies have shown that FcγRIIIa obtained through different expression systems displayed distinct N-glycan profiles leading to subtle kinetic profile variations (Hayes et al., 2017; Zeck et al., 2011). Our results suggested that these N-glycan variations modestly affected the interactions for both FcγRIIIa$_{F158}$ and FcγRIIIa$_{V158}$ (Fig. 6; Supplementary Table S1) as was observed previously (Cambay et al., 2019).

The TZM glycoforms binding to both FcγRIIIa$_{F158}$ and FcγRIIIa$_{V158}$ were affected the most by the IgG1-Fc N-glycan profiles (Fig. 6). These results are in agreement with the literature in which a major influence on all the FcγRIII isoforms (i.e., FcγRIIIa$_{F158}$, FcγRIIIa$_{V158}$, FcγRIIIb NA1 and FcγRIIIb NA2) has been reported (Dekkers et al., 2017; Subedi and Barb, 2016; Zhang et al., 2011). More precisely, variation in core fucosylation had the most radical impact on FcγRIIIa binding while no significant effect on other FcγRs was observed (Fig. 6a–e). IgG1s with low-fucose levels have been reported to form more stable complexes with FcγRIIIa, due to carbohydrate-carbohydrate interactions between the FcγRIIIa Asn-162 glycan and afucosylated IgG1-Fc (Ferrara et al., 2006b, 2011; Mizushima et al., 2011), and resulting in more efficient capability to induce an ADCC response (Dekkers et al., 2017; Wada et al., 2019; Subedi and Barb, 2016; Li et al., 2017).

In addition, the presence of galactose, independently of the core fucose, was found to benefit binding of the IgG1s to both FcγRIIIa variants (Fig. 6f and g). This combination can therefore be considered an additive advantage, which has been confirmed by several reports (Dekkers et al., 2017; Wada et al., 2019; Subedi and Barb, 2016; Houde et al., 2010) while contested by others (Peipp et al., 2008; Peschke et al., 2017). To a lesser extent, galactose, irrespective of the core fucose level, also positively influenced the interactions of TZM (Fig. 6h–j) and other IgG1s (Thomann et al., 2015; Subedi and Barb, 2016; Dashivets et al., 2015) with FcγRI, FcγRIIa and FcγRIIb.

We also showed that TZM glycovariants enriched in mono-α2,6-sialylation (Fig. 6f and g) have the same affinity as their digalactosylated counterpart (Dekkers et al., 2017; Thomann et al., 2015; Subedi and Barb, 2016; Dashivets et al., 2015). Nonetheless, a slight decrease in FcγRIIIa affinity for the di-α2,6-sialylated (40%) TZM glycoforms was observed compared to its digalactosylated counterpart. This difference is however not statistically significant and is most likely due to the disialylation levels which remained low in our preparations. This trend is in line with conclusions made in recent studies for IgG1 glycoforms displaying higher levels or complete disialylation, with this effect being observed either on fucosylated (Li et al., 2017), afucosylated (Dekkers et al., 2017; Kurogochi et al., 2015) or both forms (Wada et al., 2019). In the case of hypo-fucosylated TZMs, the effects of digalactosylation, mono- and di-sialylation were more modest than those observed for their fucosylated counterparts (Fig. 6f and g). However, it should be taken into account that the levels of afucosylation of our TZM preparations are different (i.e., fucosylation is higher for galactosylated and sialylated TZM samples compared to our agalactosylated TZM sample, see Fig. 4). These differences may be important, as demonstrated by Chung et al. (2012). In the case of the other receptors, TZM sialylation had no impact upon FcγRIIa and FcγRIIb (Fig. 6h and i), as already observed for other IgG1s (Dekkers et al., 2017; Subedi and Barb, 2016). Of interest, a modest, yet significant ($p \leq 0.01$), positive effect on FcγRI binding was observed for the fucosylated TZM samples only (Fig. 6j). Such affinity increase has already been reported by Scallon et al. (2007) but was not observed by others (Dekkers et al., 2017; Thomann et al., 2015; Subedi and Barb, 2016). Altogether, our results suggest that the TZM mono-α2,6-sialylation modestly affects its interaction with FcγRI compared to the digalactosylated variant. It also showed that disialylation has a negative effect on the TZM affinity for the FcγRIIIa when disialylation levels reaches a certain threshold (>40%). This contrasts with many studies that concluded that disialylation had no effect (Thomann et al., 2015; Subedi and Barb, 2016; Dashivets et al., 2015; Peipp et al., 2008; Shivatare et al., 2018; Lin et al., 2015) but agree with others who performed these experiments with homogenous IgG1 glycoform preparations (Wada et al., 2019; Kurogochi et al., 2015).

Altogether, the similarity in the trends observed for those TZM low-galactosylation/high-galactosylation/high-sialylation glycovariants in the absence or presence of fucose, highly suggests that both core fucosylation and elongation of the glycans affect FcγR binding through distinct mechanisms. This hypothesis is consistent with the very specific role of core fucose in the IgG1/FcγRIIIa interaction (Ferrara et al., 2011; Mizushima et al., 2011), as well as with the effect of galactose and/or sialic acid on the IgG1-Fc conformation (Ahmed et al., 2014; Frank et al., 2014).

The correlations between the IgG1/FcγR interactions and the induction of an ADCC (Dekkers et al., 2017; Thomann et al., 2015; Wada et al., 2019; Li et al., 2017; Scallon et al., 2007; Shivatare et al., 2018; Lin et al., 2015; Tsukimura et al., 2017; Zhang et al., 2011; Chung et al., 2012) and CDC (Dekkers et al., 2017; Wada et al., 2019; Peschke et al., 2017; Chung et al., 2012) response, or the overall performance of a therapeutic IgG1 *in vivo* (Kaneko et al., 2006; Li et al., 2017; Kanda et al., 2006) have already been reported. To mimic the multiple IgG1-Fc/FcγRIIIa interactions that may occur simultaneously *in vivo*, we performed a cell-based reporter bioassay in which the effector cells are engineered Jurkat cells that express either the FcγRIIIa$_{F158}$ or the FcγRIIIa$_{V158}$. In this assay, binding of an IgG1 to its target protein on the target cell allows for the interaction of their Fc region with the FcγRIIIa$_{F158}$ or FcγRIIIa$_{V158}$ expressed on the effector cell and results in the activation of the NFAT signalling cascade that is coupled to a bioluminescent read-out.

As expected, core fucosylation had a major effect, regardless of the FcγRIIIa variant (Fig. 7a–d and Supplementary Table S2). This positive effect of reduced antibody fucosylation on activity has been extensively demonstrated in ADCC assays (Dekkers et al., 2017; Yamane-Ohnuki et al., 2004; Wada et al., 2019; Peipp et al., 2008; Kurogochi et al., 2015; Tsukimura et al., 2017; Chung et al., 2012; Kanda et al., 2006). For both high- and low-fucosylated TZM glycovariants, terminal galactosylation and terminal sialylation had a modest, yet noteworthy, effect (Fig. 7a–d and Supplementary Table S2). As observed in our SPR assay, differences between the low-fucosylated forms were modest in our reporter bioassay, again most likely due to the various levels in residual fucosylation of our TZM glycovariants (see above). The impact of terminal galactosylation and terminal sialylation was obvious when the IgG1s were fucosylated (Fig. 7c and d; Supplementary Table S2) as indicated by the EC_{50} values for TZM GT (i.e., 46.31 and 25.02 ng/mL) and TZM GT ST6 IVS (i.e., 57.24 and 26.65 ng/mL) respectively, compared to EC_{50} values of TZM (i.e., 71.04 and 36.34 ng/mL). In contrast, the slightly negative effect of di-α2,6-sialylation compared to digalactosylation was modest (Fig. 7c and d; Supplementary Table S2), which is also demonstrated in the calculated EC_{50} values of TZM GT ST6 IVS compared to EC_{50} values of TZM GT (57.24 vs

46.31 and 26.65 vs 25.02 ng/mL, respectively). The positive effect of terminal galactosylation on ADCC activity has been reported in very recent studies (Dekkers et al., 2017; Thomann et al., 2015; Wada et al., 2019) but not by others (Shinkawa et al., 2003; Boyd et al., 1995; Peipp et al., 2008; Kurogochi et al., 2015; Tsukimura et al., 2017). Similarly, several studies have also reported the negative effect of di-α2,6-sialylation on ADCC activity (Dekkers et al., 2017; Wada et al., 2019; Li et al., 2017; Naso et al., 2010) whereas others showed no effect (Thomann et al., 2015; Peipp et al., 2008; Shivatare et al., 2018; Kurogochi et al., 2015; Lin et al., 2015).

Altogether, results we presented here showed that the affinities measured by SPR for a large panel of TZM glycovariants were highly predictive of conclusions drawn in our reporter bioassay. Indeed, a strong correlation was observed for the K_D values derived from our SPR analysis and the EC_{50} values derived from our reporter bioassay (Fig. 7e and f).

Conclusions

The results obtained from this study highlight the complexity of the effects of IgG1-Fc N-glycosylation, particularly terminal sialylation, on the interactions with the FcγRs. Our results for various glycoforms of TZM are in line with most of the conclusions from the recent seminal work by Dekkers and colleagues who investigated the impact of glycosylation of an anti-human RhD antibody with a different SPR assay (Dekkers et al., 2017). This complexity echoes the multiple protein-protein, protein-glycan and glycan-glycan interfaces involved as it highlights the need for a careful glycosylation characterization to fully understand the subtleties of the mechanism governing IgG1/FcγR interactions. Furthermore, this study underlines the usefulness of using SPR biosensors to predict the *in vitro,* and possibly *in vivo,* effector functions such as ADCP, CDC and the ADCC response of therapeutic antibodies.

Declaration of Competing Interest

The authors declare that they have no known competing financial interests or personal relationships that could have appeared to influence the work reported in this paper.

CRediT authorship contribution statement

Florian Cambay: Conceptualization, Methodology, Formal analysis, Visualization, Writing - original draft. **Céline Raymond:** Conceptualization, Methodology, Formal analysis, Visualization, Writing - original draft. **Denis Brochu:** Investigation, Formal analysis. **Michel Gilbert:** Investigation, Formal analysis. **The Minh Tu:** Investigation, Formal analysis. **Christiane Cantin:** Investigation, Formal analysis. **Anne Lenferink:** Supervision. **Maxime Grail:** Validation, Data curation, Validation. **Olivier Henry:** Supervision, Writing - review & editing, Funding acquisition. **Gregory De Crescenzo:** Supervision, Writing - review & editing, Funding acquisition. **Yves Durocher:** Supervision, Writing - review & editing, Funding acquisition, Project administration.

Acknowledgements

We thank Gilles Saint-Laurent, Denis L'Abbé and Christian Gervais for technical support and fruitful discussions. This work was supported by the National Research Council Canada: Human Health Therapeutics Research Centre (YD), the NSERC Discovery program (YD and GDC) the Canada Research Chair on Protein-Enhanced Biomaterials (GDC), and by the TransMedTech Institute (NanoBio Technology Platform) and its main funding partner, the Canada First Research Excellence Fund. Graphical abstract was produced using Servier Medical Art.

Appendix A. Supplementary data

Supplementary data to this article can be found online at https://doi.org/10.1016/j.crimmu.2020.06.001.

References

Ahmed, A.A., Giddens, J., Pincetic, A., Lomino, J.V., Ravetch, J.V., Wang, L.-X., Bjorkman, P.J., 2014. Structural characterization of anti-inflammatory immunoglobulin G Fc proteins. J. Mol. Biol. 426, 3166–3179. https://doi.org/10.1016/j.jmb.2014.07.006.

Alessi, D.R., Andjelkovic, M., Caudwell, B., Cron, P., Morrice, N., Cohen, P., Hemmings, B.A., 1996. Mechanism of activation of protein kinase B by insulin and IGF-1. EMBO J. 15, 6541–6551. https://doi.org/10.1002/j.1460-2075.1996.tb01045.x.

Anthony, R.M., Nimmerjahn, F., Ashline, D.J., Reinhold, V.N., Paulson, J.C., Ravetch, J.V., 2008. A recombinant IgG Fc that recapitulates the anti-inflammatory activity of IVIG. Science 320, 373. https://doi.org/10.1126/science.1154315.

Arnold, J.N., Wormald, M.R., Sim, R.B., Rudd, P.M., Dwek, R.A., 2007. The impact of glycosylation on the biological function and structure of human immunoglobulins. Annu. Rev. Immunol. 25, 21–50. https://doi.org/10.1146/annurev.immunol.25.022106.141702.

Barb, A.W., Meng, L., Gao, Z., Johnson, R.W., Moremen, K.W., Prestegard, J.H., 2012. NMR characterization of immunoglobulin G Fc glycan motion on enzymatic sialylation. Biochemistry 51, 4618–4626. https://doi.org/10.1021/bi300319q.

Bigge, J.C., Patel, T.P., Bruce, J.A., Goulding, P.N., Charles, S.M., Parekh, R.B., 1995. Nonselective and efficient fluorescent labeling of glycans using 2-amino benzamide and anthranilic acid. Anal. Biochem. 230, 229–238. https://doi.org/10.1006/abio.1995.1468.

Boyd, P.N., Lines, A.C., Patel, A.K., 1995. The effect of the removal of sialic acid, galactose and total carbohydrate on the functional activity of Campath-1H. Mol. Immunol. 32, 1311–1318. https://doi.org/10.1016/0161-5890(95)00118-2.

Bruggeman, C.W., Dekkers, G., Bentlage, A.E.H., Treffers, L.W., Nagelkerke, S.Q., Lissenberg-Thunnissen, S., Koeleman, C.A.M., Wuhrer, M., van den Berg, T.K., Rispens, T., 2017. Enhanced effector functions due to antibody defucosylation depend on the effector cell Fcγ receptor profile. J. Immunol. 1700116. https://doi.org/10.4049/jimmunol.1700116.

Bruhns, P., Iannascoli, B., England, P., Mancardi, D.A., Fernandez, N., Jorieux, S., Daëron, M., 2009. Specificity and affinity of human Fcγ receptors and their polymorphic variants for human IgG subclasses. Blood 113, 3716–3725. https://doi.org/10.1182/blood-2008-09-179754.

Cambay, F., Henry, O., Durocher, Y., De Crescenzo, G., 2019. Impact of N-glycosylation on Fcgamma receptor/IgG interactions: unravelling differences with an enhanced surface plasmon resonance biosensor assay based on coiled-coil interactions. mAbs 11, 435–452. https://doi.org/10.1080/19420862.2019.1581017.

Cartron, G., Dacheux, L., Salles, G., Solal-Celigny, P., Bardos, P., Colombat, P., Watier, H., 2002. Therapeutic activity of humanized anti-CD20 monoclonal antibody and polymorphism in IgG Fc receptor FcγRIIIa gene. Blood 99, 754–758. https://doi.org/10.1182/blood.V99.3.754.

Chung, S., Quarmby, V., Gao, X., Ying, Y., Lin, L., Reed, C., Fong, C., Lau, W., Qiu, Z.J., Shen, A., 2012. Quantitative evaluation of fucose reducing effects in a humanized antibody on Fcγ receptor binding and antibody-dependent cell-mediated cytotoxicity activities. mAbs 4, 326–340. https://doi.org/10.4161/mabs.19941.

Dashivets, T., Thomann, M., Rueger, P., Knaupp, A., Buchner, J., Schlothauer, T., 2015. Multi-angle effector function analysis of human monoclonal IgG glycovariants. PloS One 10, e0143520. https://doi.org/10.1371/journal.pone.0143520.

Dekkers, G., Plomp, R., Koeleman, C.A., Visser, R., von Horsten, H.H., Sandig, V., Rispens, T., Wuhrer, M., Vidarsson, G., 2016. Multi-level glyco-engineering techniques to generate IgG with defined Fc-glycans. Sci. Rep. 6, 36964. https://doi.org/10.1038/srep36964.

Dekkers, G., Treffers, L., Plomp, R., Bentlage, A.E.H., de Boer, M., Koeleman, C.A.M., Lissenberg-Thunnissen, S.N., Visser, R., Brouwer, M., Mok, J.Y., Matlung, H., van den Berg, T.K., van Esch, W.J.E., Kuijpers, T.W., Wouters, D., Rispens, T., Wuhrer, M., Vidarsson, G., 2017. Decoding the human immunoglobulin G-glycan repertoire reveals a spectrum of Fc-receptor- and complement-mediated-effector activities. Front. Immunol. 8, 877. https://doi.org/10.3389/fimmu.2017.00877.

Dorion-Thibaudeau, J., Raymond, C., Lattova, E., Perreault, H., Durocher, Y., De Crescenzo, G., 2014. Towards the development of a surface plasmon resonance assay to evaluate the glycosylation pattern of monoclonal antibodies using the extracellular domains of CD16a and CD64. J. Immunol. Methods 408, 24–34. https://doi.org/10.1016/j.jim.2014.04.010.

Dorion-Thibaudeau, J., St-Laurent, G., Raymond, C., De Crescenzo, G., Durocher, Y., 2016. Biotinylation of the Fc gamma receptor ectodomains by mammalian cell co-transfection: application to the development of a surface plasmon resonance-based assay. J. Mol. Recogn. 29, 60–69. https://doi.org/10.1002/jmr.2495.

Durocher, Y., Butler, M., 2009. Expression systems for therapeutic glycoprotein production. Curr. Opin. Biotechnol. 20, 700–707. https://doi.org/10.1016/j.copbio.2009.10.008.

Durocher, Y., Perret, S., Kamen, A., 2002. High-level and high-throughput recombinant protein production by transient transfection of suspension-growing human 293-EBNA1 cells. Nucleic Acids Res. 30, E9. https://doi.org/10.1093/nar/30.2.e9.

Edberg, J.C., Kimberly, R.P., 1997. Cell type-specific glycoforms of Fc gamma RIIIa (CD16): differential ligand binding. J. Immunol. 159, 3849–3857.

Ferrara, C., Brunker, P., Suter, T., Moser, S., Puntener, U., Umana, P., 2006a. Modulation of therapeutic antibody effector functions by glycosylation engineering: influence of Golgi enzyme localization domain and co-expression of heterologous beta1, 4-N-acetylglucosaminyltransferase III and Golgi alpha-mannosidase II. Biotechnol. Bioeng. 93, 851–861. https://doi.org/10.1002/bit.20777.

Ferrara, C., Stuart, F., Sondermann, P., Brunker, P., Umana, P., 2006b. The carbohydrate at FcgammaRIIIa Asn-162. An element required for high affinity binding to non-

fucosylated IgG glycoforms. J. Biol. Chem. 281, 5032–5036. https://doi.org/10.1074/jbc.M510171200.
Ferrara, C., Grau, S., Jager, C., Sondermann, P., Brunker, P., Waldhauer, I., Hennig, M., Ruf, A., Rufer, A.C., Stihle, M., Umana, P., Benz, J., 2011. Unique carbohydrate-carbohydrate interactions are required for high affinity binding between FcgammaRIII and antibodies lacking core fucose. Proc. Natl. Acad. Sci. U.S.A. 108, 12669–12674. https://doi.org/10.1073/pnas.1108455108.
Frank, M., Walker, R.C., Lanzilotta, W.N., Prestegard, J.H., Barb, A.W., 2014. Immunoglobulin G1 Fc domain motions: implications for Fc engineering. J. Mol. Biol. 426, 1799–1811. https://doi.org/10.1016/j.jmb.2014.01.011.
Hayes, J.M., Frostell, A., Karlsson, R., Muller, S., Martin, S.M., Pauers, M., Reuss, F., Cosgrave, E.F., Anneren, C., Davey, G.P., Rudd, P.M., 2017. Identification of Fc gamma receptor glycoforms that produce differential binding kinetics for rituximab. Mol. Cell. Proteomics 16, 1770–1788. https://doi.org/10.1074/mcp.M117.066944.
Houde, D., Peng, Y., Berkowitz, S.A., Engen, J.R., 2010. Post-translational modifications differentially affect IgG1 conformation and receptor binding. Mol. Cell. Proteomics 9, 1716–1728. https://doi.org/10.1074/mcp.M900540-MCP200.
Jefferis, R., 2009. Recombinant antibody therapeutics: the impact of glycosylation on mechanisms of action. Trends Pharmacol. Sci. 30, 356–362. https://doi.org/10.1016/j.tips.2009.04.007.
Jiang, X.-R., Song, A., Bergelson, S., Arroll, T., Parekh, B., May, K., Chung, S., Strouse, R., Mire-Sluis, A., Schenerman, M., 2011. Advances in the assessment and control of the effector functions of therapeutic antibodies. Nat. Rev. Drug Discov. 10, 101–111. https://doi.org/10.1038/nrd3365.
Kanda, Y., Yamada, T., Mori, K., Okazaki, A., Inoue, M., Kitajima-Miyama, K., Kuni-Kamochi, R., Nakano, R., Yano, K., Kakita, S., 2006. Comparison of biological activity among nonfucosylated therapeutic IgG1 antibodies with three different N-linked Fc oligosaccharides: the high-mannose, hybrid, and complex types. Glycobiology 17, 104–118. https://doi.org/10.1093/glycob/cwl057.
Kaneko, Y., Nimmerjahn, F., Ravetch, J.V., 2006. Anti-inflammatory activity of immunoglobulin G resulting from Fc sialylation. Science 313, 670–673. https://doi.org/10.1126/science.1129594.
Kelly, R.M., Kowle, R.L., Lian, Z., Strifler, B.A., Witcher, D.R., Parekh, B.S., Wang, T., Frye, C.C., 2018. Modulation of IgG1 immunoeffector function by glycoengineering of the GDP-fucose biosynthesis pathway. Biotechnol. Bioeng. 115, 705–718. https://doi.org/10.1002/bit.26496.
Kurogochi, M., Mori, M., Osumi, K., Tojino, M., Sugawara, S.-I., Takashima, S., Hirose, Y., Tsukimura, W., Mizuno, M., Amano, J., 2015. Glycoengineered monoclonal antibodies with homogeneous glycan (M3, G0, G2, and A2) using a chemoenzymatic approach have different affinities for FcγRIIIa and variable antibody-dependent cellular cytotoxicity activities. PloS One 10, e0132848. https://doi.org/10.1371/journal.pone.0132848.
Lalonde, M.-E., Durocher, Y., 2017. Therapeutic glycoprotein production in mammalian cells. J. Biotechnol. 251, 128–140. https://doi.org/10.1016/j.jbiotec.2017.04.028.
Lee, E.U., Roth, J., Paulson, J.C., 1989. Alteration of terminal glycosylation sequences on N-linked oligosaccharides of Chinese hamster ovary cells by expression of beta-galactoside alpha 2, 6-sialyltransferase. J. Biol. Chem. 264, 13848–13855.
Li, T., DiLillo, D.J., Bournazos, S., Giddens, J.P., Ravetch, J.V., Wang, L.-X., 2017. Modulating IgG effector function by Fc glycan engineering. Proc. Natl. Acad. Sci. U.S.A. 114, 3485–3490. https://doi.org/10.1073/pnas.1702173114.
Lin, C.-W., Tsai, M.-H., Li, S.-T., Tsai, T.-I., Chu, K.-C., Liu, Y.-C., Lai, M.-Y., Wu, C.-Y., Tseng, Y.-C., Shivatare, S.S., 2015. A common glycan structure on immunoglobulin G for enhancement of effector functions. Proc. Natl. Acad. Sci. U.S.A. 112, 10611–10616. https://doi.org/10.1073/pnas.1513456112.
Lu, J., Chu, J., Zou, Z., Hamacher, N.B., Rixon, M.W., Sun, P.D., 2015. Structure of FcgammaRI in complex with Fc reveals the importance of glycan recognition for high-affinity IgG binding. Proc. Natl. Acad. Sci. U.S.A. 112, 833–838. https://doi.org/10.1073/pnas.1418812112.
Mizushima, T., Yagi, H., Takemoto, E., Shibata-Koyama, M., Isoda, Y., Iida, S., Masuda, K., Satoh, M., Kato, K., 2011. Structural basis for improved efficacy of therapeutic antibodies on defucosylation of their Fc glycans. Gene Cell. 16, 1071–1080. https://doi.org/10.1111/j.1365-2443.2011.01552.x.
Naso, M.F., Tam, S.H., Scallon, B.J., Raju, T.S., 2010. Engineering host cell lines to reduce terminal sialylation of secreted antibodies. mAbs 2, 519–527. https://doi.org/10.4161/mabs.2.5.13078.
Peipp, M., van Bueren, J.J.L., Schneider-Merck, T., Bleeker, W.W.K., Dechant, M., Beyer, T., Repp, R., van Berkel, P.H.C., Vink, T., van de Winkel, J.G.J., 2008. Antibody fucosylation differentially impacts cytotoxicity mediated by NK and PMN effector cells. Blood 112, 2390–2399. https://doi.org/10.1182/blood-2008-03-144600.
Peschke, B., Keller, C.W., Weber, P., Quast, I., Lünemann, J.D., 2017. Fc-galactosylation of human immunoglobulin gamma isotypes improves C1q binding and enhances complement-dependent cytotoxicity. Front. Immunol. 8, 646. https://doi.org/10.3389/fimmu.2017.00646.
Raju, T.S., 2008. Terminal sugars of Fc glycans influence antibody effector functions of IgGs. Curr. Opin. Immunol. 20, 471–478. https://doi.org/10.1016/j.coi.2008.06.007.
Raju, T.S., Briggs, J.B., Chamow, S.M., Winkler, M.E., Jones, A.J.S., 2001. Glycoengineering of therapeutic glycoproteins: in vitro galactosylation and sialylation of glycoproteins with terminal N-acetylglucosamine and galactose residues. Biochemistry 40, 8868–8876. https://doi.org/10.1021/bi010475i.
Raymond, C., Robotham, A., Kelly, J., Lattova, E., Perreault, H., Durocher, Y., 2012. Production of highly sialylated monoclonal antibodies. In: Petrescu, S. (Ed.), Glycosylation, IntechOpen Publisher. https://doi.org/10.5772/51301.
Raymond, C., Robotham, A., Spearman, M., Butler, M., Kelly, J., Durocher, Y., 2015. Production of alpha2,6-sialylated IgG1 in CHO cells. mAbs 7, 571–583. https://doi.org/10.1080/19420862.2015.1029215.
Rillahan, C.D., Antonopoulos, A., Lefort, C.T., Sonon, R., Azadi, P., Ley, K., Dell, A., Haslam, S.M., Paulson, J.C., 2012. Global metabolic inhibitors of sialyl-and fucosyltransferases remodel the glycome. Nat. Chem. Biol. 8, 661–668. https://doi.org/10.1038/nchembio.999.
Royle, L., Radcliffe, C.M., Dwek, R.A., Rudd, P.M., 2007. Detailed structural analysis of N-glycans released from glycoproteins in SDS-PAGE gel bands using HPLC combined with exoglycosidase array digestions. Glycobiol. Protoc. 125–143. https://doi.org/10.1385/1-59745-167-3:125.
Scallon, B.J., Tam, S.H., McCarthy, S.G., Cai, A.N., Raju, T.S., 2007. Higher levels of sialylated Fc glycans in immunoglobulin G molecules can adversely impact functionality. Mol. Immunol. 44, 1524–1534. https://doi.org/10.1016/j.molimm.2006.09.005.
Shields, R.L., Lai, J., Keck, R., O'Connell, L.Y., Hong, K., Meng, Y.G., Weikert, S.H.A., Presta, L.G., 2002. Lack of fucose on human IgG1 N-linked oligosaccharide improves binding to human FcγRIII and antibody-dependent cellular toxicity. J. Biol. Chem. 277, 26733–26740. https://doi.org/10.1074/jbc.M202069200.
Shinkawa, T., Nakamura, K., Yamane, N., Shoji-Hosaka, E., Kanda, Y., Sakurada, M., Uchida, K., Anazawa, H., Satoh, M., Yamasaki, M., 2003. The absence of fucose but not the presence of galactose or bisecting N-acetylglucosamine of human IgG1 complex-type oligosaccharides shows the critical role of enhancing antibody-dependent cellular cytotoxicity. J. Biol. Chem. 278, 3466–3473. https://doi.org/10.1074/jbc.M210665200.
Shivatare, S.S., Huang, L.-Y., Zeng, Y.-F., Liao, J.-Y., You, T.-H., Wang, S.-Y., Cheng, T., Chiu, C.-W., Chao, P., Chen, L.-T., 2018. Development of glycosynthases with broad glycan specificity for the efficient glyco-remodeling of antibodies. Chem. Commun. 54 (48), 6161–6164. https://doi.org/10.1039/C8CC03384F.
Subedi, G.P., Barb, A.W., 2016. The immunoglobulin G1 N-glycan composition affects binding to each low affinity Fc gamma receptor. mAbs 8, 1512–1524. https://doi.org/10.1080/19420862.2016.1218586.
Subedi, G.P., Barb, A.W., 2018. CD16a with oligomannose-type N-glycans is the only "low-affinity" Fc gamma receptor that binds the IgG crystallizable fragment with high affinity in vitro. J. Biol. Chem. 293, 16842–16850. https://doi.org/10.1074/jbc.RA118.004998.
Thomann, M., Schlothauer, T., Dashivets, T., Malik, S., Avenal, C., Bulau, P., Ruger, P., Reusch, D., 2015. In vitro glycoengineering of IgG1 and its effect on Fc receptor binding and ADCC activity. PloS One 10. https://doi.org/10.1371/journal.pone.0134949.
Tsukimura, W., Kurogochi, M., Mori, M., Osumi, K., Matsuda, A., Takegawa, K., Furukawa, K., Shirai, T., 2017. Preparation and biological activities of anti-HER2 monoclonal antibodies with fully core-fucosylated homogeneous bi-antennary complex-type glycans. Biosci. Biotechnol. Biochem. 81, 2353–2359. https://doi.org/10.1080/09168451.2017.1394813.
van Berkel, P.H.C., Gerritsen, J., van Voskuilen, E., Perdok, G., Vink, T., van de Winkel, J.G.J., Parren, P.W.H.I., 2010. Rapid production of recombinant human IgG with improved ADCC effector function in a transient expression system. Biotechnol. Bioeng. 105, 350–357. https://doi.org/10.1002/bit.22535.
von Horsten, H.H., Ogorek, C., Blanchard, V., Demmler, C., Giese, C., Winkler, K., Kaup, M., Berger, M., Jordan, I., Sandig, V., 2010. Production of non-fucosylated antibodies by co-expression of heterologous GDP-6-deoxy-D-lyxo-4-hexulose reductase. Glycobiology 20, 1607–1618. https://doi.org/10.1093/glycob/cwq109.
Wada, R., Matsui, M., Kawasaki, N., 2019. Influence of N-glycosylation on effector functions and thermal stability of glycoengineered IgG1 monoclonal antibody with homogeneous glycoforms. mAbs 11, 350–372. https://doi.org/10.1080/19420862.2018.1551044.
Walsh, G., 2018. Biopharmaceutical benchmarks 2018. Nat. Biotechnol. 36, 1136–1145. https://doi.org/10.1038/nbt.4305.
Yamaguchi, Y., Nishimura, M., Nagano, M., Yagi, H., Sasakawa, H., Uchida, K., Shitara, K., Kato, K., 2006. Glycoform-dependent conformational alteration of the Fc region of human immunoglobulin G1 as revealed by NMR spectroscopy. Biochim. Biophys. Acta Gen. Subj. 1760, 693–700. https://doi.org/10.1016/j.bbagen.2005.10.002.
Yamane-Ohnuki, N., Kinoshita, S., Inoue-Urakubo, M., Kusunoki, M., Iida, S., Nakano, R., Wakitani, M., Niwa, R., Sakurada, M., Uchida, K., Shitara, K., Satoh, M., 2004. Establishment of FUT8 knockout Chinese hamster ovary cells: an ideal host cell line for producing completely defucosylated antibodies with enhanced antibody-dependent cellular cytotoxicity. Biotechnol. Bioeng. 87, 614–622. https://doi.org/10.1002/bit.20151.
Yu, X., Baruah, K., Harvey, D.J., Vasiljevic, S., Alonzi, D.S., Song, B.-D., Higgins, M.K., Bowden, T.A., Scanlan, C.N., Crispin, M., 2013. Engineering hydrophobic protein–carbohydrate interactions to fine-tune monoclonal antibodies. J. Am. Chem. Soc. 135, 9723–9732. https://doi.org/10.1021/ja4014375.
Zeck, A., Pohlentz, G., Schlothauer, T., Peter-Katalinic, J., Regula, J.T., 2011. Cell type-specific and site directed N-glycosylation pattern of FcgammaRIIIa. J. Proteome Res. 10, 3031–3039. https://doi.org/10.1021/pr1012653.
Zhang, J., Liu, X., Bell, A., To, R., Baral, T.N., Azizi, A., Li, J., Cass, B., Durocher, Y., 2009. Transient expression and purification of chimeric heavy chain antibodies. Protein Expr. Purif. 65, 77–82. https://doi.org/10.1016/j.pep.2008.10.011.
Zhang, N., Liu, L., Dan Dumitru, C., Cummings, N.R.H., Cukan, M., Jiang, Y., Li, Y., Li, F., Mitchell, T., Mallem, M.R., 2011. Glycoengineered Pichia produced anti-HER2 is comparable to trastuzumab in preclinical study. mAbs 3, 289–298. https://doi.org/10.4161/mabs.3.3.15532.